Scale of pluton/wall rock interaction near May Lake, Yosemite National Park, California, USA

Ryan Douglas Mills

A thesis submitted to the faculty of the University of North Carolina at Chapel Hill in partial fulfillment of the requirements for the degree of Master of Science in the Department of Geological Sciences.

Chapel Hill
2007

Approved by:

Advisor: Dr. Allen Glazner

Reader: Dr. Drew Coleman

Reader: Dr. Mike Oskin

ABSTRACT

RYAN DOUGLAS MILLS: Scale of pluton/wall rock interaction near May Lake, Yosemite National Park, California, USA

(Under the direction of Dr. Allen F. Glazner and Dr. Drew S. Coleman)

The western outer granodiorite of the Tuolumne Intrusive Suite intruded a variety of metasedimentary wall rocks at 93.1 ± 0.1 Ma. The May Lake metamorphic screen (4500 x 550 m) is a remnant of the chemically diverse metasedimentary host rocks. Their chemical contrast with the invading pluton provides an excellent location to study pluton/wall rock interactions.

Outside the screen, visible wall-rock xenoliths (mostly pelitic quartzite) are predominantly located in an elongate horizon surrounded by a hybridized fine-grained granodiorite. Initial Sr and Nd isotopic ratios of the hybridized granodiorite indicate incorporation of crustal material. Major- and trace-element geochemical data indicate contamination of the granodiorite with pelitic metasedimentary rocks occurred in two modes, selective assimilation of 1) a high-K partial-melt derived from pelitic quartzite, and 2) a low-K partial-melt derived from pelitic quartzite. However, there is little evidence for contamination of granodiorite beyond the immediate vicinity of wall rock inclusions.

ACKNOWLEDGEMENTS

I am thankful for the academic support I received from Dr. Allen Glazner and Dr. Drew Coleman. Their detailed knowledge of the Sierra Nevada batholith was incredibly valuable during this project. I also want to thank several graduate students; Breck Johnson, Jesse Davis, and Russ Mapes. Breck and Jesse assisted with field work in California and Russ taught and assisted me with isotope geochemistry at UNC.

Funding for this thesis was provided by the Martin Research Fund (University of North Carolina), the Bartlett Fund (University of North Carolina), and the White Mountain Research Station (University of California). The Yosemite National Park service staff provided instrumentation and permits to the park.

In addition, I am very thankful for the support I received from my entire family throughout this project.

TABLE OF CONTENTS

Page

LIST OF TABLES

LIST OF FIGURES

Introduction

Assimilation of wall rock material is commonly invoked as a cause of large-scale chemical heterogeneity in igneous rocks (McBirney et al. 1987; Clarke et al. 1998; Barnes et al. 2005; Dungan 2005) and as a space-creating mechanism for plutons in the upper crust via stoping and disaggregation (Paterson et al. 1996). Assimilation is an umbrella term that encapsulates both bulk incorporation of wall rock (bulk assimilation) and incorporation of partial melts of wall rocks, leaving behind a restitic residue (selective assimilation). These end-member mechanisms of assimilation produce different trends of chemical hybridization in plutons. Studies have defined hybridized aureoles or zones in plutons (Barnes et al. 2004; Saito et al. 2007), but few detailed, meter-scale geochemical studies have identified the assimilated material and quantified the spatial extent of contamination.

Wall rock xenoliths are rare in most plutons (typically <<1% of overall volume; Glazner and Bartley 2006); thus for incorporation of wall rocks to be a significant mass-transfer process, assimilation of crustal material must be pervasive. Because bulk assimilation of wall rocks is a thermodynamically unrealistic mechanism for pluton emplacement (Bowen 1928; Glazner 2007), Beard et al. (2005) suggested that plutons may dissolve and disperse up to 50% of their total mass during ascent and emplacement via a process known as reactive bulk assimilation, but they did not address the exact thermal budget involved in such a process. However, the chemical results of such a process would be identical to bulk assimilation.

Assimilation is detectable because it drives the composition of the magma toward the contaminant. If the contaminant is similar in composition to the magma, then little change results. If it is another igneous rock, then the contaminated magma will have an igneous composition as well. But if the contaminant is a non-igneous rock, then the contaminated magma will likely lie off of the well-defined igneous trend in compositional space (Fig. 1). In addition, whole-rock radiogenic isotopic analysis can detect assimilation if the contaminant is isotopically distinct.

This study examines chemical and physical interactions between a pluton and its wall rocks in order to place realistic limits on assimilation processes. We focus on the contact between granodiorite and metamorphic wall rocks at May Lake in Yosemite National Park, California (Figs. 2 and 3), where there are abundant glaciated outcrops, great lithologic diversity of metasedimentary rocks in the wall rock screen, and significant chemical and isotopic contrasts between the pluton and the metasedimentary rocks.

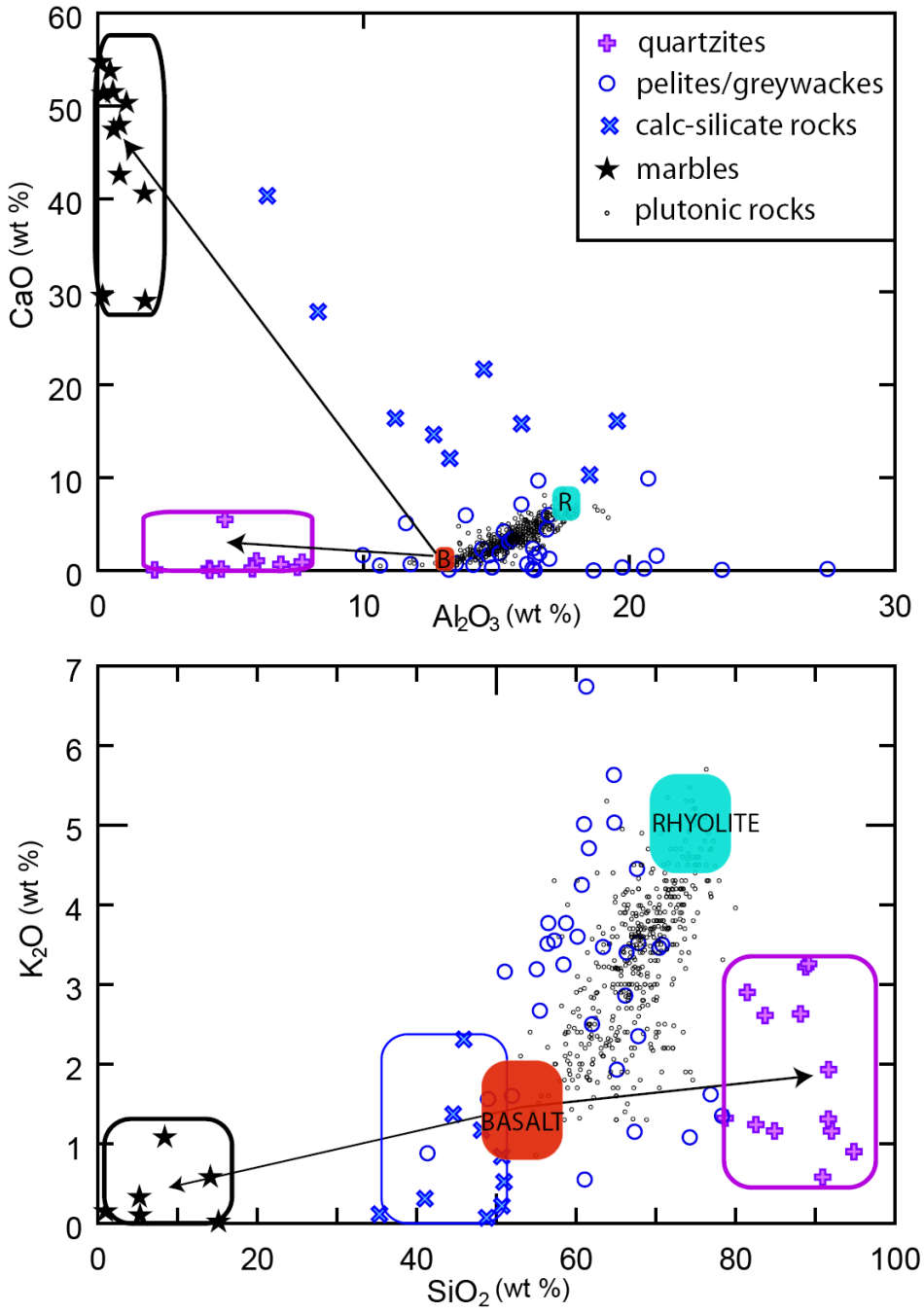

Fig.1. Selected major-element variation diagrams of plutonic rocks (Bateman et al. 1988, Gray 2003) and a variety of metasedimentary rocks (Clarke 1908, this study). The basalt and rhyolite fields show the end-member compositions of igneous rocks. Straight lines indicate mixing paths of the basalt with quartzite or marble.

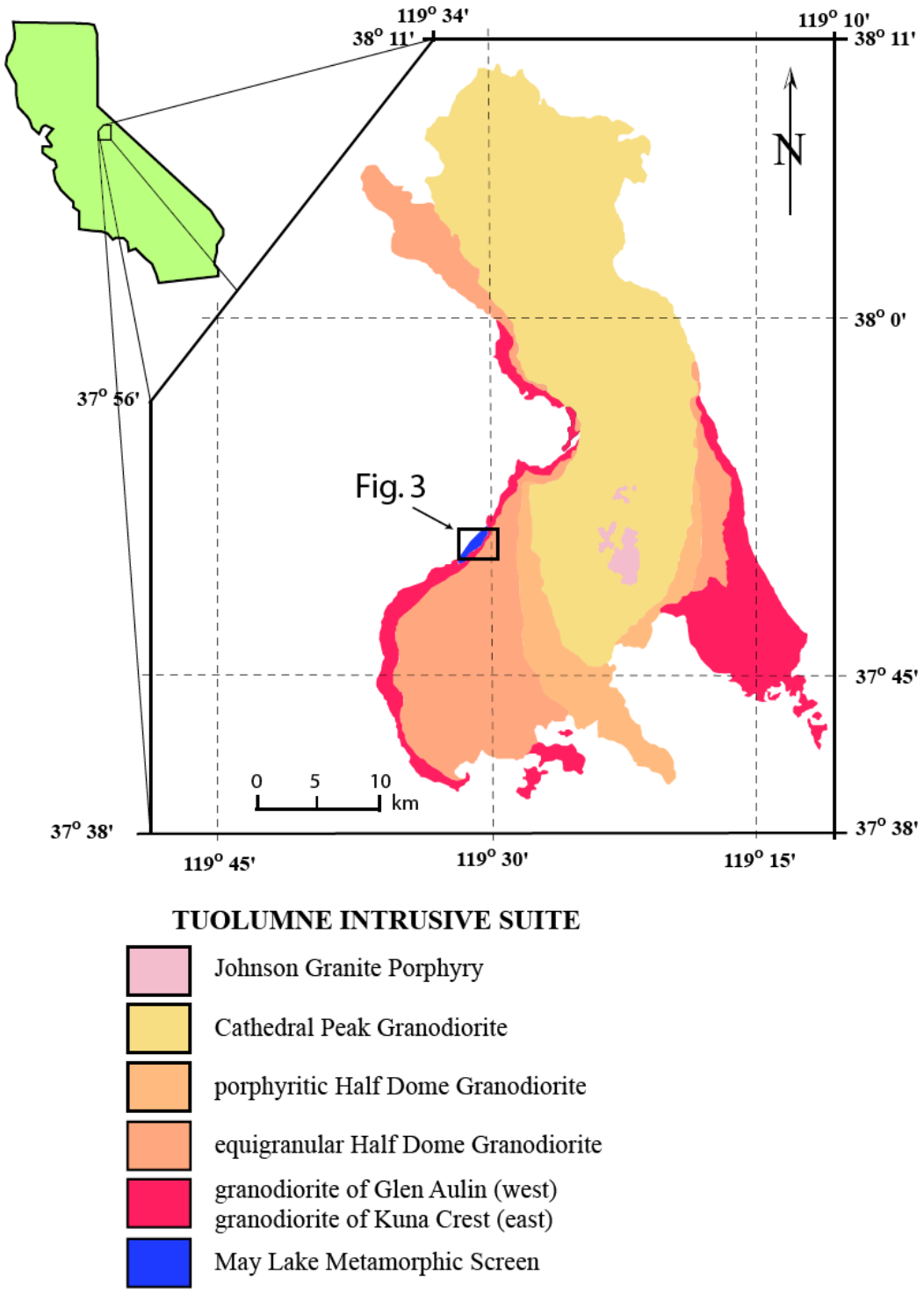

Fig. 2. Geologic map of the Tuolumne Intrusive Suite (after Huber et al 1989).

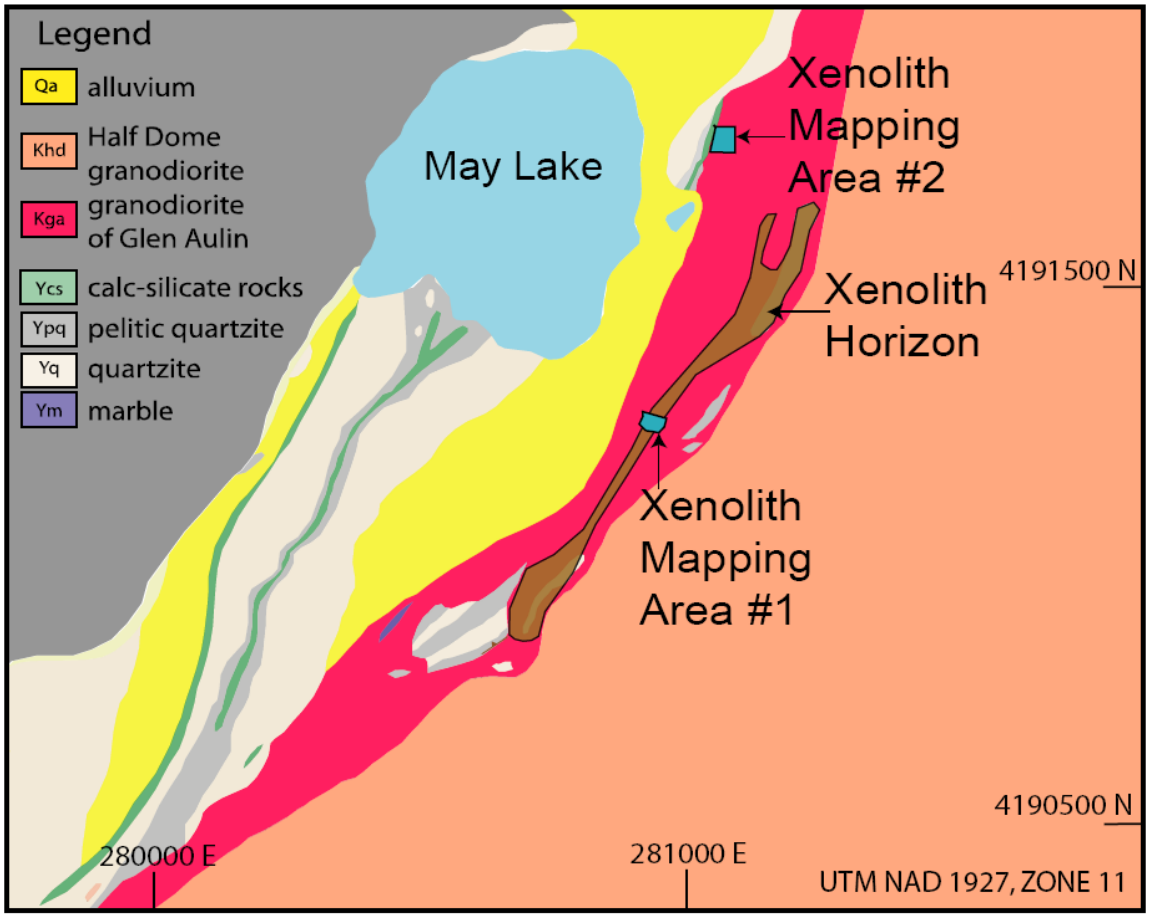

Fig. 3. Geologic map of the May Lake Metamorphic Screen (after Taylor 2003).

Geologic Background

The Tuolumne Intrusive Suite (Fig. 2) is a concentrically zoned set of plutons located in the Sierra Nevada batholith of California. The suite, which grades from a granodiorite/ tonalite at the margin to granodiorite in intermediate zones and granite porphyry at the core, was emplaced between 93.5 - 85.4 m.y. ago (Coleman et al. 2004). From margin to core $^{87}Sr/^{86}Sr_{(i)}$ values rise from 0.7058 to 0.7066 and $\varepsilon Nd_{(t)}$ values vary from -3 to -6, with the most significant isotopic changes occurring near the margins of the suite (Kistler et al. 1986; Gray 2003).

The May Lake metamorphic screen consists of metasedimentary rocks in contact with the western border phases of the Tuolumne Intrusive Suite (here referred to as granodiorite of Glen Aulin, Kga) for approximately 4 km (Figs. 2 and 3). The screen, mapped in detail by Rose (1957) and Taylor (2003), consists of quartzite, pelitic quartzite, marble, and calc-silicate rocks that are correlated with late Proterozoic units of the Mojave Desert region (Schweickert and Lahren 1991). Lahren et al. (1990) proposed that this assemblage of rocks originated far to the south and was transported ~400 km north along the proposed Mojave-Snow Lake fault.

Light gray to white quartzite makes up a majority of exposed metamorphic rocks in the screen and is primarily recrystallized quartz (85 – 95%; Rose 1957) with minor biotite and potassium feldspar. Pelitic quartzite is a foliated rock with layers of relatively pure quartzite and pelitic hornfels; layer thickness typically ranges from millimeters to meters. Biotite and muscovite define a foliation in the pelitic layers and plagioclase and

potassium feldspar are the other main components. Minor phases in the pelitic quartzite include andalusite, sillimanite, and orthopyroxene (Taylor 2003). In addition, several accessory minerals are present including apatite, zircon, monazite, and opaque minerals (Rose 1957).

The two other main metasedimentary rock types in the screen are calcareous and are present as boudins inside the quartzites. The calc-silicate rock unit is an equigranular mixture of diopside, actinolite, calcite and quartz (Taylor 2003). The marble unit is coarse-grained calcite with minor diopside and actinolite (Taylor 2003). All metasedimentary rock units show evidence for pre- and syn-emplacement deformation including several episodes of folding and boudinage (Taylor 2003; Coleman et al. 2005).

The outer unit of the Tuolumne Intrusive Suite is referred to collectively as the granodiorite of Kuna Crest (Kk), but along the western edge of the suite near May Lake, the unit is specifically referred to as the tonalite of Glen Aulin (Kga). Because these rocks plot predominantly in the granodiorite field on a QAP ternary diagram (Fig. 3) the terminology used here will be granodiorite of Glen Aulin (Kga). The granodiorite is equigranular with equant biotite defining a subtle planar fabric. Hornblende and opaque minerals are the other major mafic phases and minor sericitation of potassium feldspar is present. Plagioclase and potassium feldspar (An_{35-45} and Or_{90}; Gray 2003), along with quartz, are the main felsic constituents.

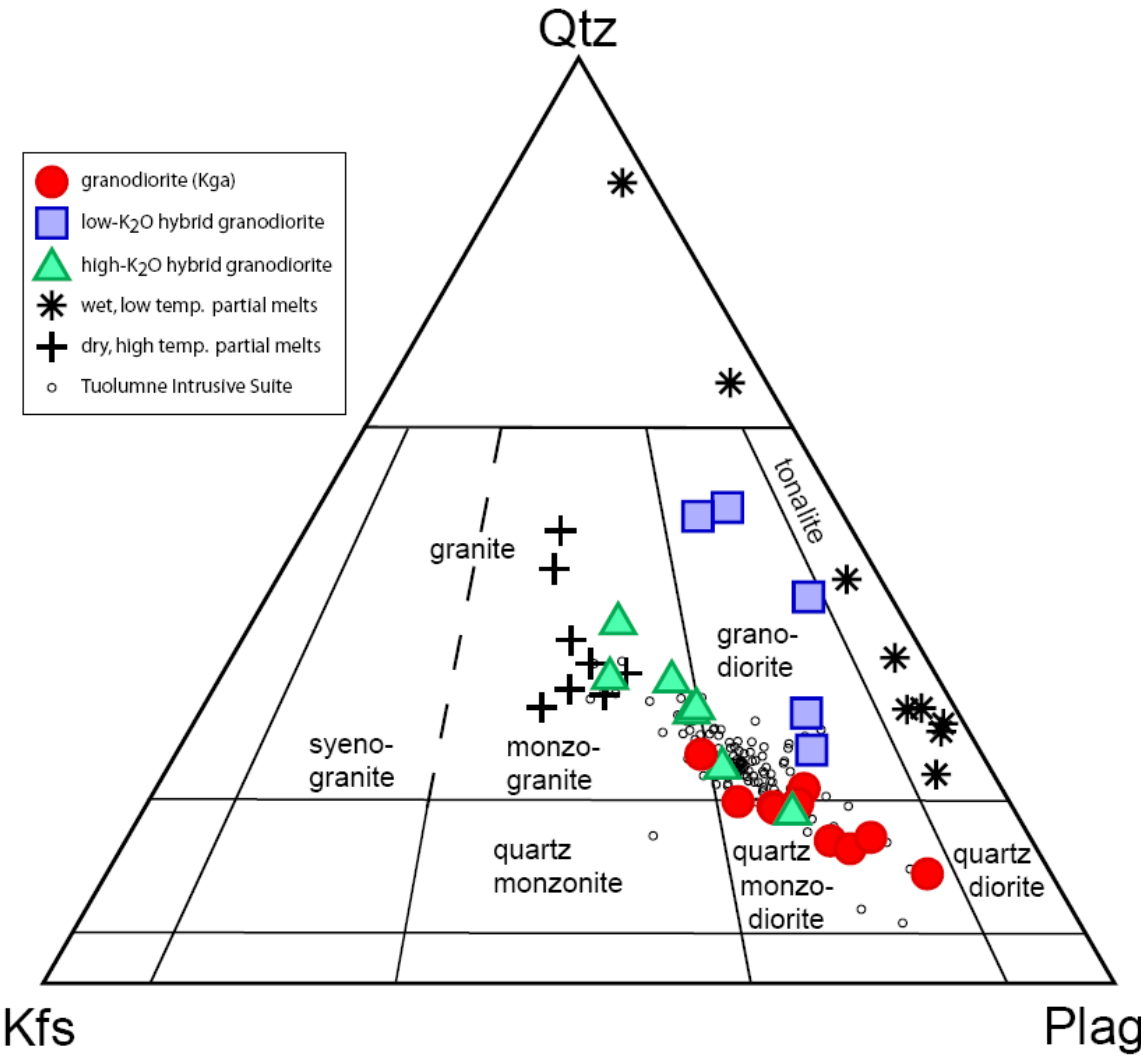

Fig. 4. Modal Quartz-Plagioclase-Potassium Feldspar compositions of plutonic rock, partial melt (Holtz and Johannes 1991; Patiño-Douce and Johnston 1991; Montel and Vielzeuf 1997; Patiño-Douce and Harris 1998) and leucosome geochemistry (Bea et al. 1994; Whitney and Irving 1994; Carrington and Watt 1995; Symmes and Ferry 1995; Zeng et al. 2005a) determined using CIPW norm algorithm. Albite compositions only contribute to the plagioclase component. Rock type classifications are after La Maitre (2002).

Methods

Sampling strategy

Sampling was focused largely within 10 meters of the contact between the May Lake screen and the granodiorite of Glen Aulin in order to understand the scale of pluton/wall rock interactions. Previously analyzed samples of the granodiorite away from the contact were also used to define the background chemistry of the unit. Samples of each wall rock unit were collected for analysis as potential pluton contaminants. A variety of granodiorite samples was collected from within 10 meters of the contact, and 2 line traverses extending perpendicular from the contact were sampled to establish the length scale of contamination.

Xenolith mapping

Two representative areas (Fig. 2) were established for detailed mapping of xenoliths in the granodiorite: one inside a particularly xenolith-rich horizon, and the other in an area with a typically low density of xenoliths. A Nikon total station was used to map the location of all visible xenoliths in the areas larger than 1 cm in longest dimension. The long and short axis dimensions and rock type were noted for each xenolith within the areas.

Geochemistry

Samples were ground to a powder using a steel jaw crusher and a ceramic shatterbox. Powders were then shipped to Activation Labratories (Ontario, Canada), for major- and trace-element analyses. Samples were dissolved by lithium metaborate/tetraborate fusion. Major-elements and Sc, Be, V, Sr, Zr, and Ba were analyzed by ICP-OES and all other trace-elements were analyzed by ICP-MS.

Isotope geochemistry

Whole-rock powder was dissolved and cations were separated for isotopic analysis following methods outlined by Miller et al. (1995). Strontium and Nd isotopic abundances were obtained on a VG Sector 54 thermal ionization mass spectrometer at the University of North Carolina at Chapel Hill. Strontium isotopic ratios were normalized to $^{86}Sr/^{88}Sr = 0.1194$ and referenced to $^{87}Sr/^{86}Sr = 0.710269$ (NBS 987, n = 4); Nd isotopic ratios were normalized to $^{146}Nd/^{144}Nd = 0.7219$ and referenced to $^{143}Nd/^{144}Nd = 0.512117$ (JNdi-metal, n = 4). Isotope dilution using spikes was not performed because Rb, Sr, Sm and Nd concentrations were obtained via ICP-MS. $^{87}Sr/^{86}Sr_{(i)}$ and $\varepsilon Nd_{(t)}$ indicate values corrected to 93.1 Ma, the crystallization age of the granodiorite (Coleman et al. 2004). Epsilon values for Nd were calculated using $^{143}Nd/^{144}Nd(CHUR, 0\ Ma) = 0.512638$ and $^{147}Sm/^{144}Nd(CHUR, 0\ Ma) = 0.1967$.

Heavy mineral separates

100 g blocks of 3 samples (ML051.02, ML051.03, & ML061.63) were reduced to sand size using a Bico disc mill. Highly magnetic minerals were removed from the

samples with a hand magnet. Remaining minerals were passed through methelyne iodide with a density of 3.32 g/cm^3 to segregate dense minerals. Heavy mineral separates were mounted in epoxy, polished, and identified using energy-dispersive x-ray analysis on a Leica SEM with special attention to rare earth element- (REE) and Th-bearing phases.

Results

Field relationships

The May Lake screen is approximately 4500 meters in length and 550 meters in width. Each of the four major metasedimentary rock units is locally in contact with the granodiorite but only pelitic quartzite, the only foliated metasedimentary unit, displays evidence of concordant dike injections resulting in isolation of metasedimentary blocks (Fig. 4a).

Xenoliths in the granodiorite around May Lake occur predominantly in a tabular zone. The zone is approximately 1100 meters long and 200 meters wide and strikes subparallel to the contact of the screen and granodiorite. Xenoliths in the zone range in size from a few square centimeters to a single, large block, 140 meters by 240 meters, near the contact (Taylor 2003). Hybridized, fine-grained granodiorite surrounds most xenoliths in the tabular xenolith zone (Fig. 4b) and the hybridized granodiorite has a lower abundance of mafic minerals than the typical granodiorite. Xenoliths found in the hybridized zone are chiefly pelitic quartzite and show more ductile deformation than xenoliths outside of the zone. Granodiorite immediately surrounding the xenolith zone has modally layered bands defined by mafic minerals parallel to the edge of the zone (Fig. 4c). In contrast, xenolith-free zones of the granodiorite have little to no modal layering.

Mapping of xenoliths in the xenolith horizon illustrates the contrast between the horizon and surrounding granodiorite. Mapping area #1 (Fig. 3, Fig. 5) consisted of a 40

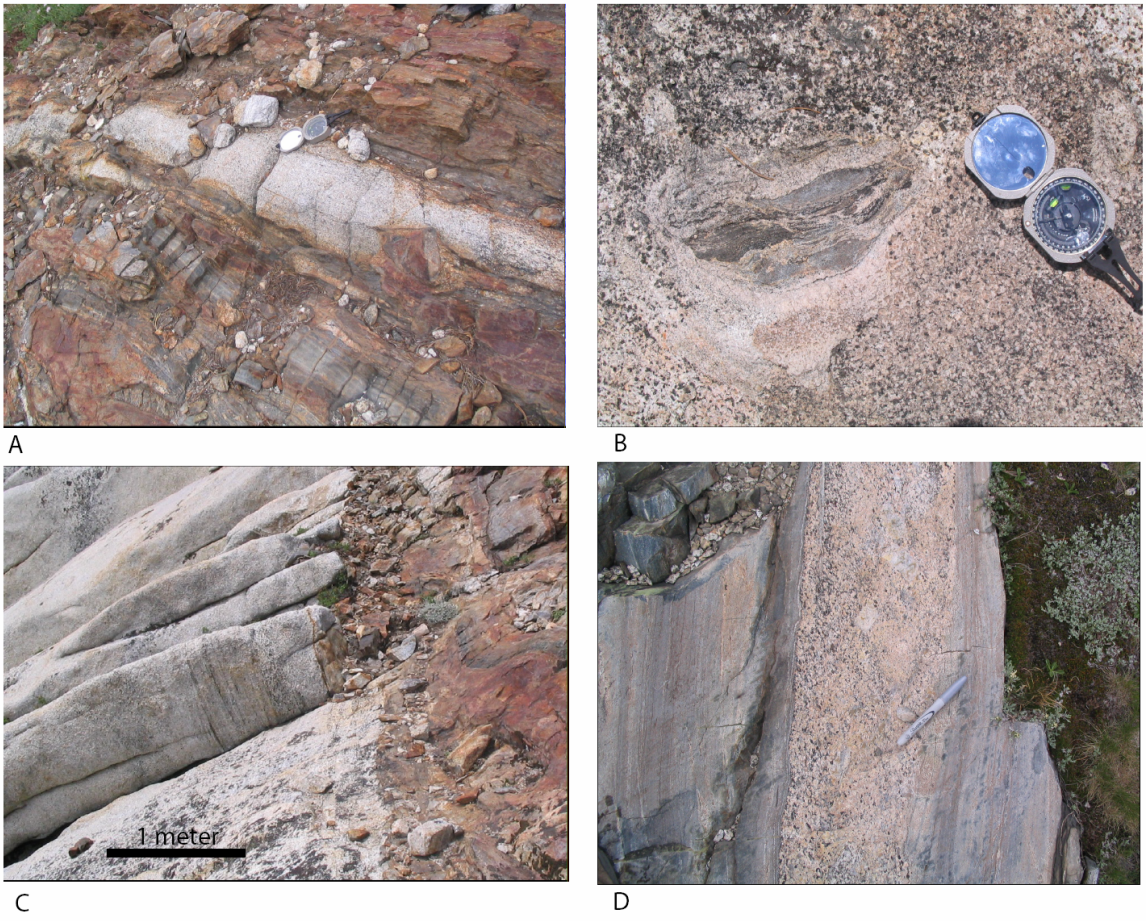

Fig. 5. Field photographs of interactions between plutonic rocks and metamorphic wall rocks. Photograph A shows a concordant intrusion of hybridized granodiorite in the pelitic quartzite. Photograph B shows a pelitic quartzite xenolith surrounded by a leucocratic rind. Photograph C shows a contact between granodiorite and a large block of mixed metasedimentary rock type. Modal layering in the granodiorite is prominent parallel to the block contact. Photograph D shows a concordant intrusion of granodiorite in foliated metavolcanic rocks on the eastern side of the suite.

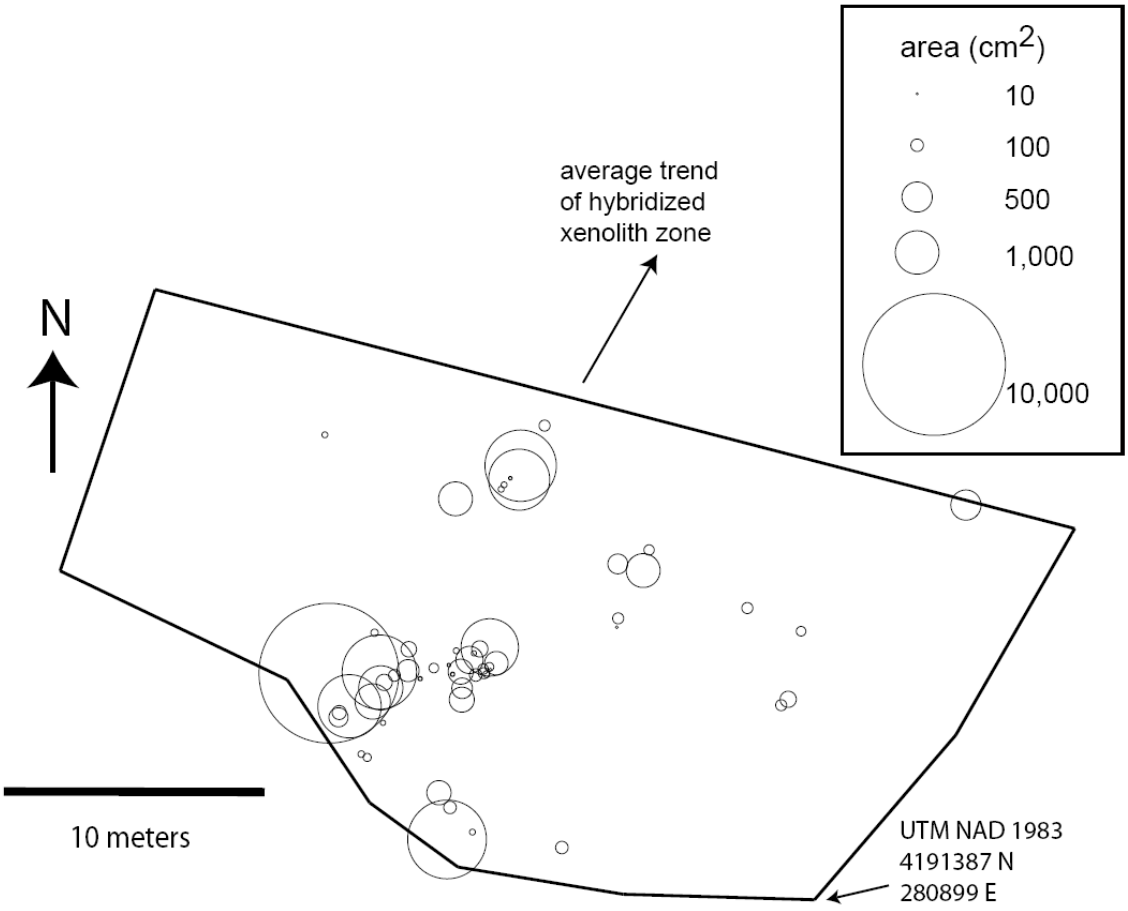

Fig. 6. Representation of xenoliths mapped in zone 1. Circles are proportional to xenolith area, elliptical area calculated from long and short axis field measurements.

meter x 20 meter area of excellent exposure chosen to encompass the xenolith-rich horizon. The xenolith-rich horizon is approximately 10-15 m thick and is surrounded by typical xenolith-poor granodiorite. Although xenoliths account for ~2.5% of the 800 m^2 area surveyed, within the xenolith-rich horizon in this mapping area, xenoliths make up 10.5% by area, illustrating the subjectivity of quantifying xenolith abundances. In the second mapping area (Fig. 3), adjacent to the contact with calc-silicate rocks, xenoliths make up 0.005% of the 1050 m^2 area, with all xenoliths occurring within 10 m of the contact.

Major- and trace-element geochemistry

Major and trace-element data are presented in Table 1. Plutonic rock samples with Sr and Nd isotopic ratios within the range of values from previously reported standard Kga samples (Kistler 1986; Gray 2003) are denoted "granodiorite." Plutonic rock samples with $^{87}Sr/^{86}Sr_{(i)}$ values higher than standard Kga and $\varepsilon Nd_{(t)}$ values more negative than standard Kga are denoted "hybridized granodiorite."

Among granodiorite samples all major-element concentrations (Fig. 7) negatively correlate with SiO_2 (55–68 wt. %) except K_2O, which correlates positively, and Na_2O, which shows no correlation. Rubidium, Ba, and Zr correlate positively with SiO_2, whereas Sr, Zn, V, and Sc negatively correlate. Rare-earth element concentrations for granodiorite normalized to chondrite show slight light rare earth element (LREE) enrichment with values averaging ~100 times chondrite for La (Fig. 8). A few samples show minor positive and negative Eu anomalies, but as a whole, the granodiorite has only minor Eu anomalies.

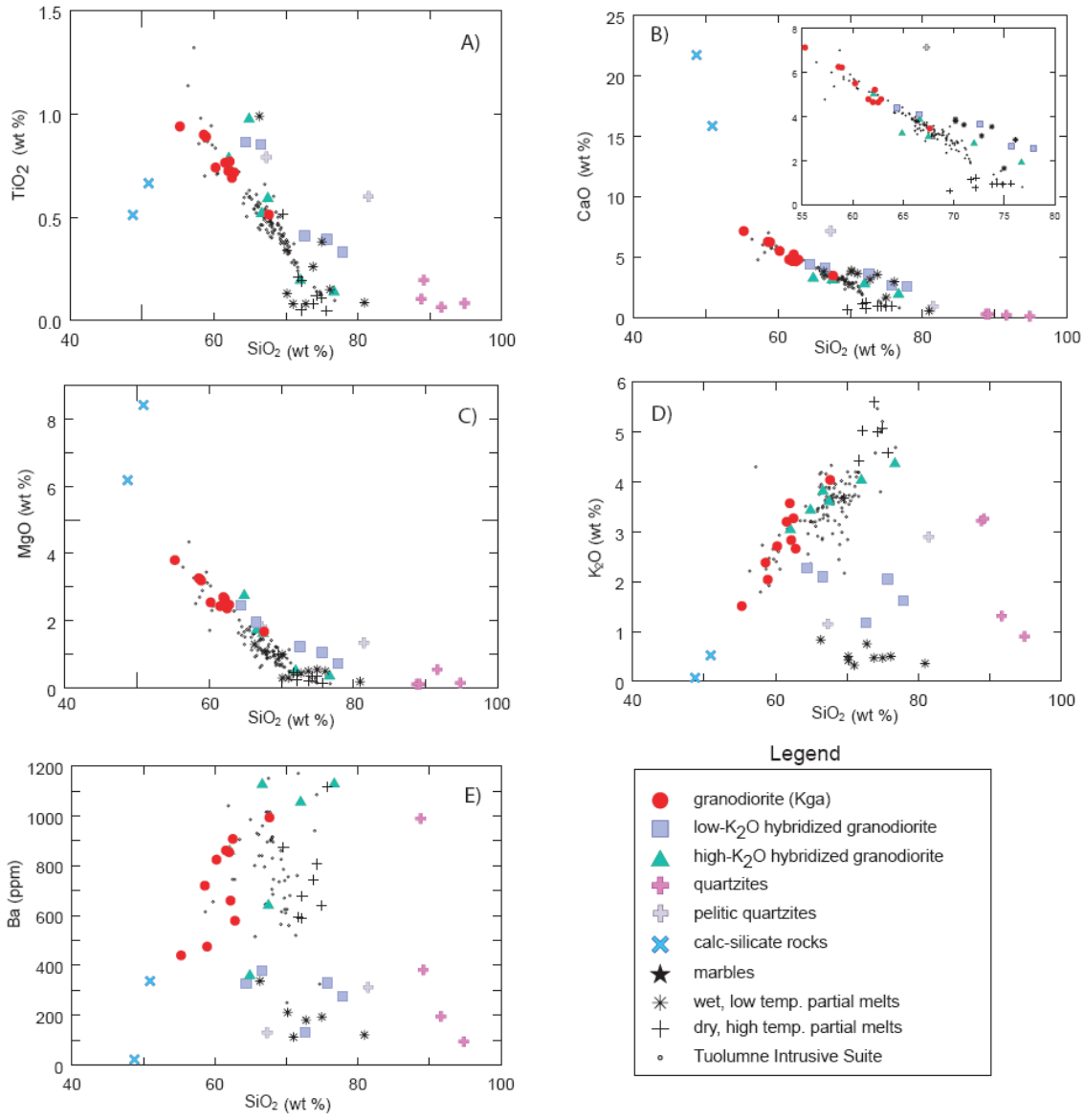

Fig. 7. Selected major- and trace-element variation diagrams of: 1) plutonic and metamorphic rocks near May Lake, 2) experimental partial melting data (Holtz and Johannes 1991; Patiño-Douce and Johnston 1991; Montel and Vielzeuf 1997; Patiño-Douce and Harris 1998), 3) leucosome geochemistry (Bea et al. 1994; Whitney and Irving 1994; Carrington and Watt 1995; Symmes and Ferry 1995; Zeng et al. 2005a), and 4) plutonic rock geochemistry of Tuolumne Intrusive Suite (Bateman et al. 1988, Gray 2003).

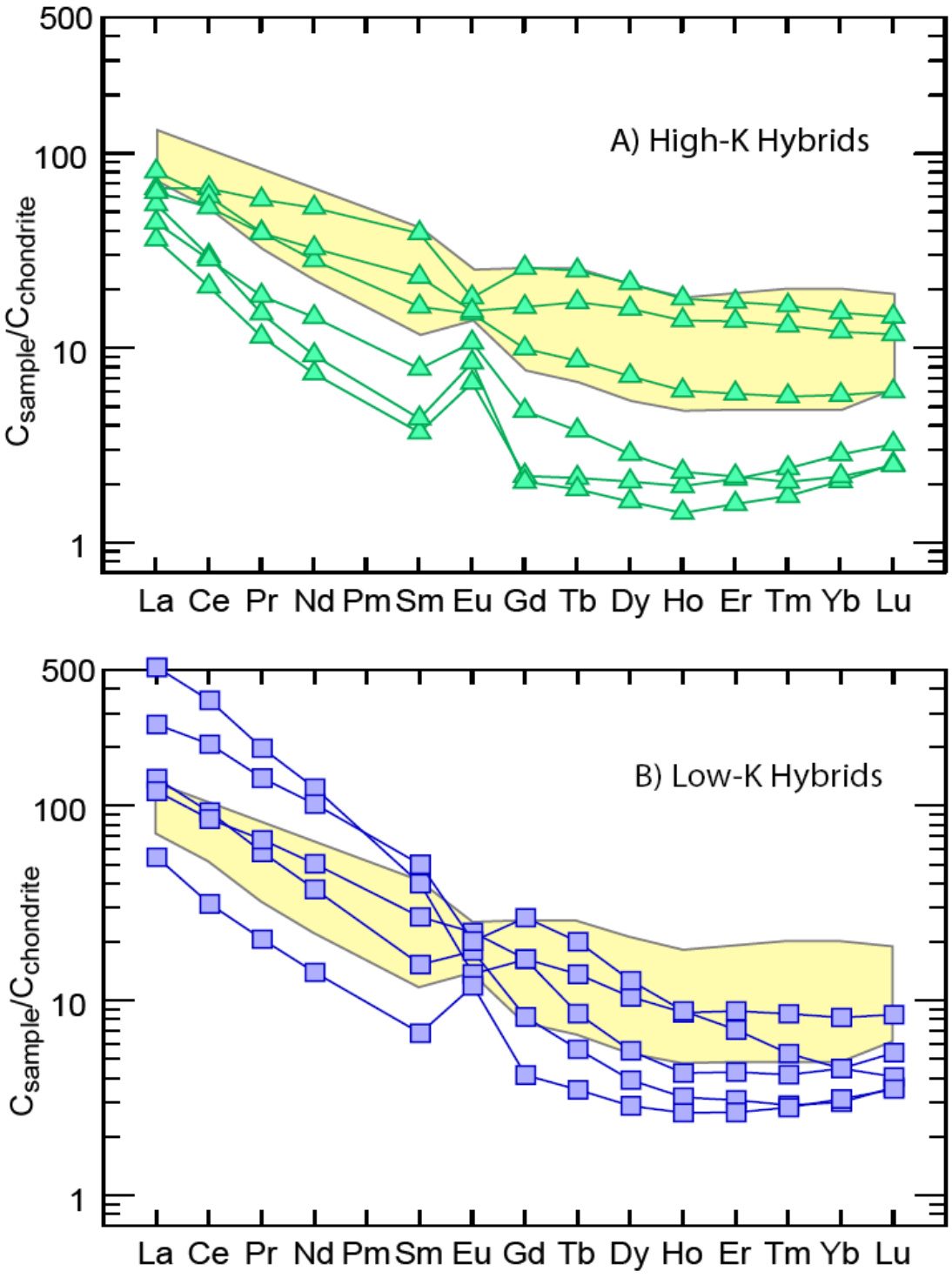

Fig. 8. Rare-earth element geochemistry of plutonic rocks plotted relative to chondrite (Sun and McDonough 1989). Plot A displays the high-K hybridized samples and plot B displays the low-K hybridized samples. Shaded area in the background represents Kga samples (Gray, 2003; this study).

Most hybridized granodiorite samples have higher concentrations of SiO_2 (62–78 wt. %) than granodiorite samples and diverge into two groups when correlated with K_2O. Group A (hereafter referred to as high-K) has a positive correlation between SiO_2 and K_2O, following the trend of the entire Tuolumne Intrusive Suite. Group B (hereafter referred to as low-K) has a negative correlation between SiO_2 and K_2O, and K_2O concentrations are predominantly <2 wt. % for rocks in this group. Barium concentrations (Fig. 7e) differ between groups, with high-K samples having high Ba concentrations (~1000 ppm) and low-K samples having lower Ba concentrations (<400 ppm). Low-K samples can have higher LREE concentrations (Figs.8, 9) than high-K and granodiorite samples. Several of the hybridized samples have large Eu anomalies, some positive and some negative, but there is no correlation between the groups defined by K_2O concentrations and the sign or intensity of Eu anomalies.

Metasedimentary rocks found in the screen span a large range of major-element compositions. The quartzite has measured SiO_2 values between 88–95 wt. % with variable amounts of Al_2O_3 and K_2O making up most of the remainder. Outcrops of the quartzite are massive with weak foliation, in contrast to the well-foliated pelitic quartzite. The composition of the pelitic quartzite varies depending on the relative abundance of silt to sand layers in the protolith, with SiO_2 ranging from 67–81 wt. %. The calc-silicate rock unit has SiO_2 concentrations around 50 wt. % and 6–9 wt. % MgO. The marble varies in purity, but both analyzed samples have ~48 wt. % unnormalized CaO.

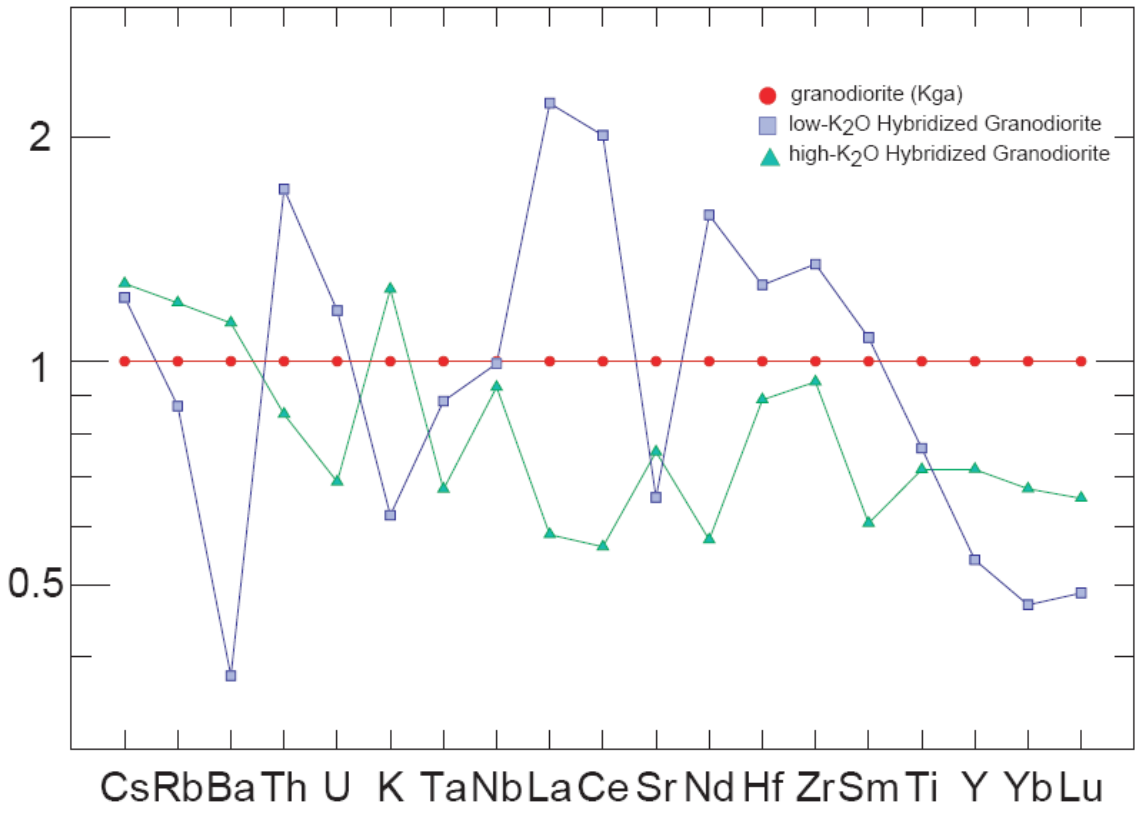

Fig. 9. Trace-element variation diagram displaying averages of the low-K_2O hybrids and high-K_2O hybrids normalized relative to the average of the normal granodiorite. The two groups of hybrids exhibit major differences for trace-elements such as Ba, Th, and all REE. Concentrations of hybridized trace-elements approach the normal granodiorite with decreasing levels of contamination.

Sr and Nd isotope geochemistry

Whole-rock Nd and Sr isotope ratios are presented in Table 2. $^{87}Sr/^{86}Sr_{(i)}$ and $\varepsilon Nd_{(t)}$ are corrected to the crystallization age of the granodiorite of Glen Aulin (93.1 Ma). Granodiorite away from the screen exhibits a range of $\varepsilon Nd_{(t)}$ from -3.43 to -3.78 and $^{87}Sr/^{86}Sr_{(i)}$ from 0.705795 to 0.705935 (Kistler 1986; Gray 2003; this study). Hybridized granodiorite ranges in $\varepsilon Nd_{(t)}$ from -3.54 to -10.46 and $^{87}Sr/^{86}Sr_{(i)}$ from 0.706105 to 0.714147, and $\varepsilon Nd_{(t)}$ and $^{87}Sr/^{86}Sr_{(i)}$ correlate throughout the hybridized granodiorite samples (Fig. 10). All granodiorite samples with hybridized compositions were collected within 2 meters of wall rock material and all samples farther from the wall rocks show no isotopic variation from the granodiorite. Plots of distance from wall rock vs. isotopic ratios (Fig. 11) show the dramatic decrease in isotopic heterogeneity as distance from wall rock increases. A plot of $\varepsilon Nd_{(t)}$ versus K_2O (Fig. 12) clearly differentiates the two contamination trends in the hybridized granodiorite samples, with one contaminant having high K_2O (~5 wt. %) and the other contaminant having low K_2O (<1 wt. %).

The potential contaminants all have more radiogenic Sr isotopic ratios and less radiogenic Nd isotopic ratios than the granodiorite, with $\varepsilon Nd_{(t)}$ ranging from -7.92 to -23.65 for both types of quartzites, and approximately equal to -18 for calc-silicate rocks, and -16 for marbles. The variability in isotopic ratios and daughter isotope whole-rock concentrations produces a great variety of potential mixing trends between the granodiorite and varied metasedimentary wall rocks.

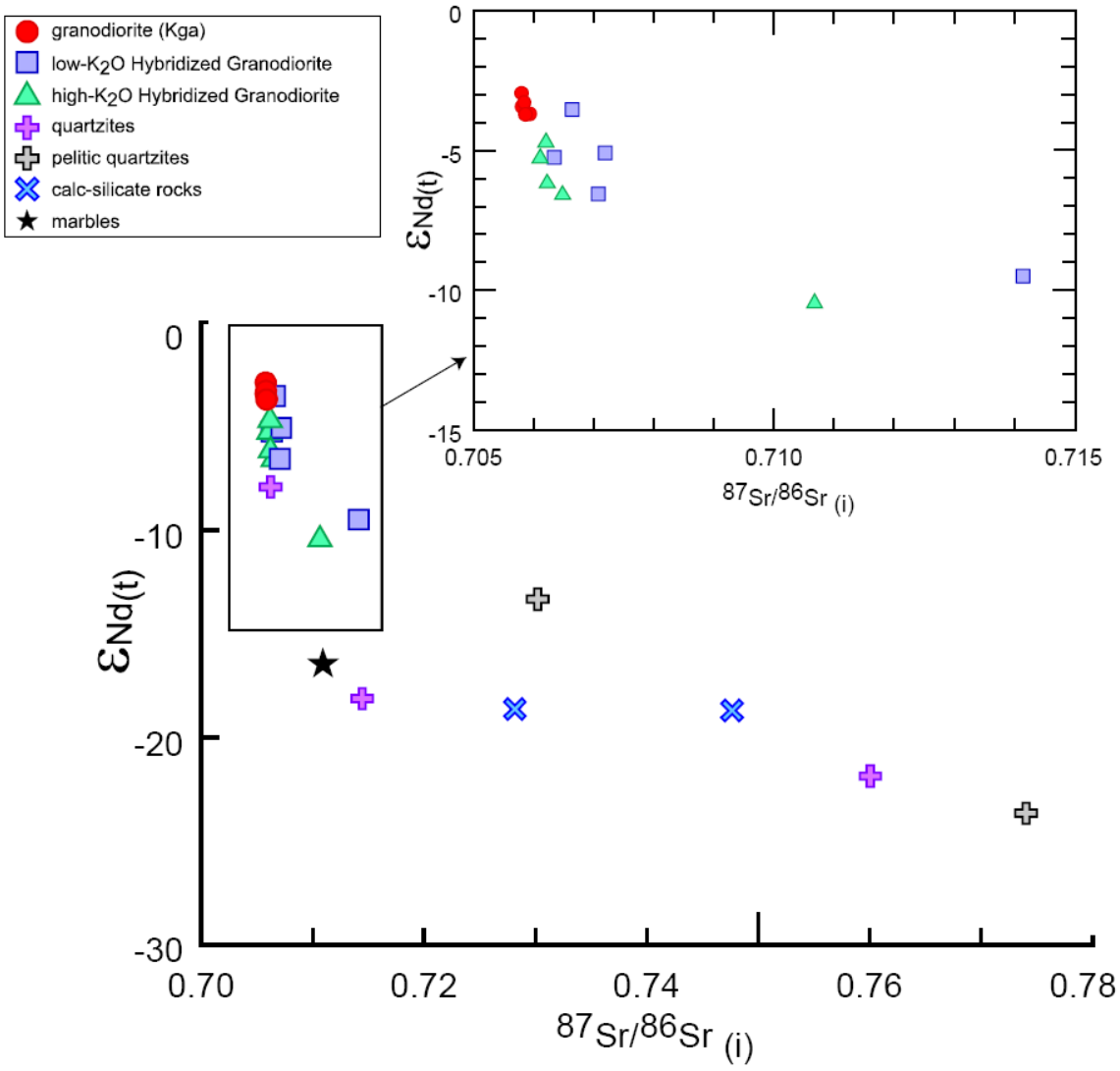

Fig. 10. Plot of $\varepsilon Nd_{(t)}$ against $^{87}Sr/^{86}Sr_{(i)}$, both corrected to 93.1 Ma. Wall rocks span a large isotopic range whereas granodiorite samples define a small range. The hybridized samples spread from the granodiorite toward the wall rocks.

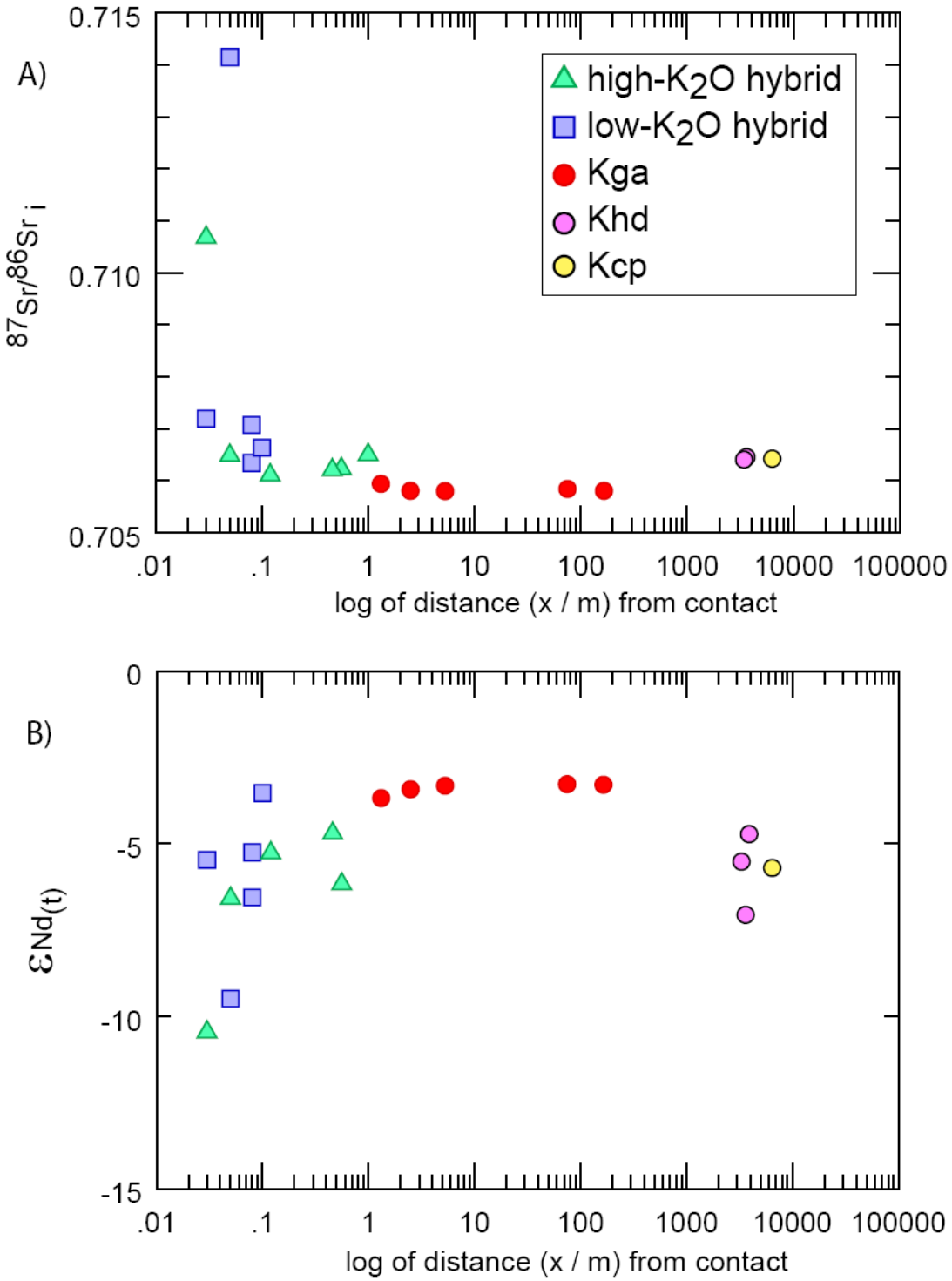

Fig. 11. Plot A and B show the isotopic variability of Sr and Nd in the plutonic rocks relative to distance from wall rock material. Selected inner unit samples with the May Lake metamorphic screen as their closest wall rock are also plotted.

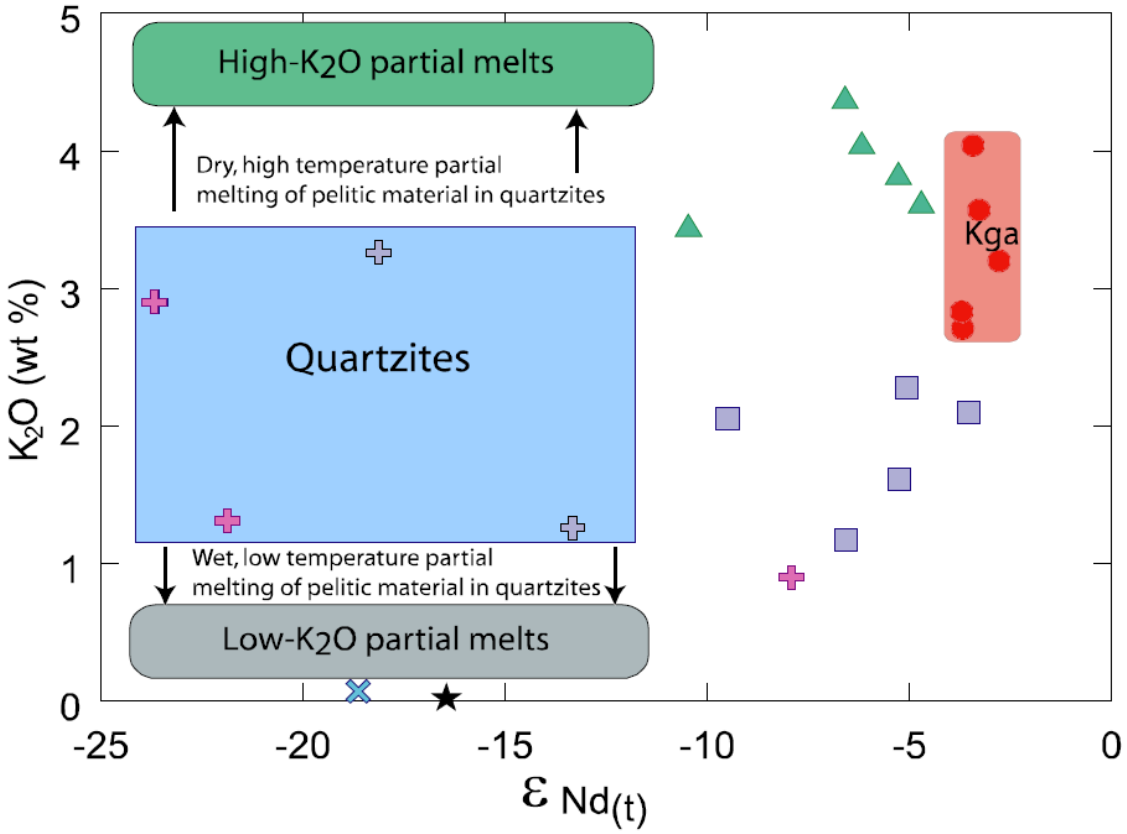

Fig. 12. Plot of $\varepsilon Nd_{(t)}$ corrected to 93.1 Ma versus K_2O (wt %) illustrating two trends in contamination of Kga. One trend has increased K_2O as $\varepsilon Nd_{(t)}$ gets more negative and the other has decreased K_2O as $\varepsilon Nd_{(t)}$ gets more negative. Partial melting can produce two distinct chemical compositions while $\varepsilon Nd_{(t)}$ stays relatively constant, because these melting reactions do not significantly fractionate Sm from Nd.

Trace mineralogy

Semi-quantitative observations of heavy mineral separates are summarized in Table 3. Monazite is the only observed phase in the pelitic quartzite sample (ML051.03) with stoichiometric concentrations of LREE and Th. Allanite is the only observed phase with stoichiometric concentrations of LREE in the plutonic rock samples and uranothorite is the only observed phase with stoichiometric concentrations of Th in the plutonic rock samples. However, the relative abundances of allanite and thorite are higher in the hybridized sample (ML051.02) than they are in the granodiorite sample (ML061.63). Although monazite, allanite, and uranothorite have the highest concentrations of LREE and Th, the remaining minerals of the rock house the majority of these elements.

Mixing percentages

Weighted least-squares analysis of major-element concentrations was performed to estimate percentages of the granodiorite component and the contaminant component in the hybridized samples. Average major-element concentrations of Kga were used as one end-member of mixing and averages of partial melting experimental data and leucosome analyses (divided into low-K and high-K groups) were used as the other end-members of mixing. The low-K_2O contaminant was used for hybridized samples that have lower K_2O weight percents than the granodiorite and the high-K_2O contaminant was used for hybridized samples that have higher K_2O weight percents than the granodiorite. Calculations for individual hybridized samples produced mixing percentages ranging

from 15% wall rock contaminated to ~100% wall rock contaminated (Fig. 13), with highly contaminated samples occurring within 10 centimeters of the wall rock.

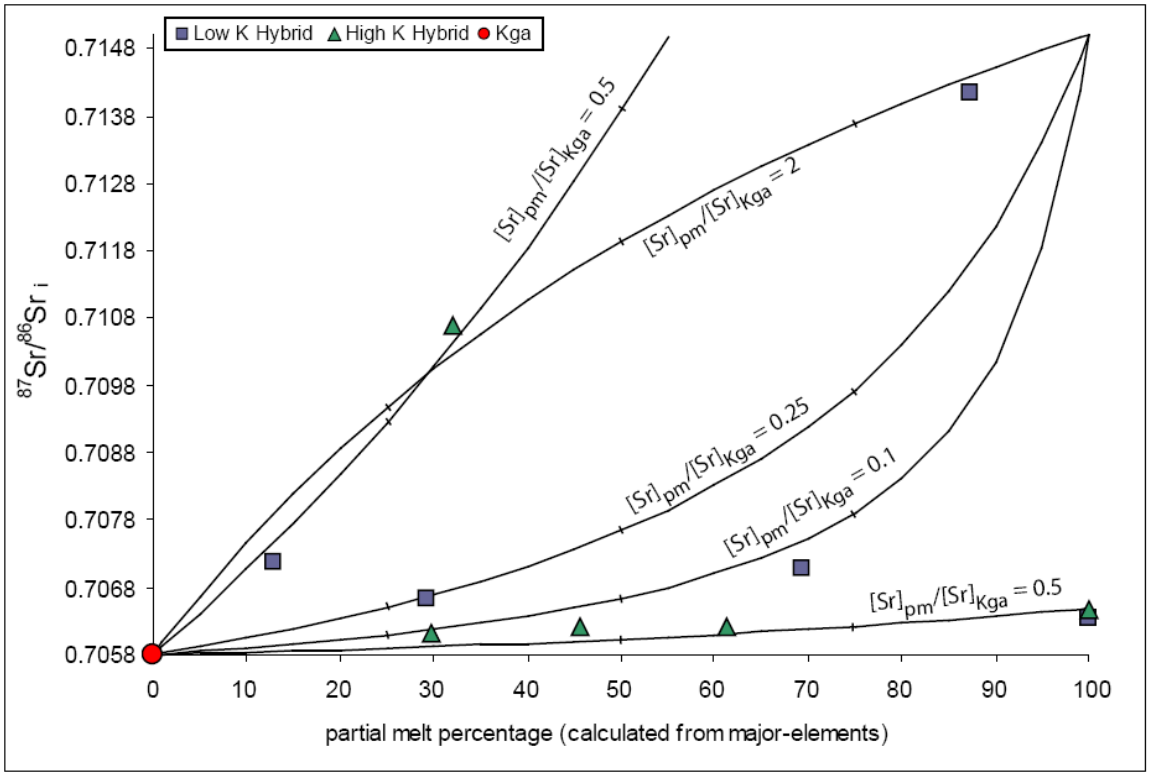

Fig. 13. $^{87}Sr/^{86}Sr_i$ values for average Kga and hybridized granodiorite samples plotted against results from weighted least-squares mixing analysis of major-element chemistry. Mixing hyperbolas for several wall rock partial melt scenarios are shown to illustrate: 1) the variability in isotopic ratio of the quartzites in the screen (shown are 3 examples: 0.730, 0.715, and 0.765), and 2) the variability in mixing paths dependent on Sr concentrations in the partial melts. Tick marks on the mixing paths represent 25%, 50%, and 75%.

Discussion

Xenoliths

Xenoliths observed in the granodiorite are overwhelmingly pelitic quartzite (~90%, determined from xenolith mapping) and metamorphic residue interpreted as restite from pelitic quartzite based on major- and trace-element geochemistry. However, the metasedimentary screen contains only ~5 area % pelitic quartzite, the remaining ~95 area % consisting of massive wall rock units (quartzite, marble, calc-silicate rocks; Fig. 3) as estimated from Taylor's (2003) map of the area. Thus, observed xenolith abundances do not conform to wall rock abundances in the May Lake screen. Physical properties of the wall rock such as foliation, and chemical properties such as mineral fertility for partial melting, play an important role in determining what rock types the magma body incorporated as xenoliths.

Incorporation of the pelitic quartzite into the magma occurred via brittle fracture along foliated layers, by dehydration melting reactions in muscovite and biotite-rich layers of the pelitic quartzite, or by a combination of the two processes. The pelitic quartzite is the only foliated unit in the May Lake screen, but foliated metavolcanic rocks in contact with the eastern margin of the Tuolumne Intrusive Suite experienced similar separation and incorporation along metamorphic foliation (Fig. 5d).

Wall rock xenoliths are concentrated in a planar horizon (Fig. 3) oriented subparallel to the contact between the screen and the pluton. Surrounding most xenoliths in the horizon is a fine-grained, leucocratic, hybridized granodiorite that appears to be a

mixture of granodiorite and felsic material from the xenoliths (Fig. 5b). The hybridized granodiorite is restricted to within a few meters of visible pelitic material. The horizon suggests syn-emplacement disaggregation, dispersal, and partial melting of wall rock blocks by pulses of magma that later hybridized.

Although the pelitic quartzites are chemically diverse, the sample taken from a xenolith in the horizon (ML051.09) shows some evidence of being restitic material. Silica content in the xenolith is significantly lower (59 wt. %) than the measured values from the pelitic quartzite in the screen (67 and 81 wt. %). The Rb/Sr ratio is anomalously low (0.09 vs. 0.56 and 4.1 in the screen), consistent with removal of incompatible elements during partial melting. These observations are consistent with findings by Verplanck et al. (1999) for restitic xenoliths of Precambrian granite wall rocks in the Organ Needle Pluton, New Mexico, and by Preston et al. (1999) and their modeled chemical composition for pelite restite after extraction of a rhyolitic partial melt.

Determining contaminants

The variability found in the hybridized granodiorite geochemical data, and specifically the bimodal K_2O trends (Figs. 7 and 12), suggest incorporation of a minimum of two different contaminants. One contamination trend produced hybrid samples that have a positive correlation between K_2O and SiO_2. Bulk assimilation of the observed wall rocks in the screen (marble, calc-silicate rocks, quartzite, and pelitic quartzite) cannot produce the major-element variability seen in these high-K hybrids. All geochemical data for these rocks suggest contamination by a rhyolitic partial melt derived from the wall rocks. The second contamination trend has a negative correlation between K_2O and SiO_2.

Major-element data for this trend fit either bulk assimilation of pure quartzite, or selective assimilation of a low-K_2O partial melt derived from the wall rocks.

The low-K hybridized granodiorites have significant trace-element variability, including large variations in Th and LREE. Two samples (ML051.02 and ML061.36) have concentrations of Th and REE that are significantly higher than any granodiorite or quartzite sample. For these samples, hybridization was not a result of bulk assimilation of pure quartzite. The remaining low-K hybrids do not show this dramatic spike in Th or LREE and thus bulk assimilation of pure quartzite is plausible according to chemical analyses. However, if the low-K trend is produced from one distinct contamination process, then the low-K hybrids with the largest chemical variability highlight the assimilation process and the low-K hybrids with mild chemical variability exemplify the same process cryptically. Overall, evidence for bulk assimilation of quartz is plausible in a few mildly hybridized samples.

Because selective assimilation of partial melts derived from wall rocks is the likely contaminant for both K_2O trends of hybridization (high-K and low-K), it is important to determine the parental wall rock for the melts. Partial melting generally results in a liquid with different chemistry than the original solid. Because the pure quartzite and marble units are essentially monomineralic rocks, they are extremely limited in their ability to melt incongruently, and would only produce minimal volumes of partial melt. This restricts potential fertile source rocks from the screen that could produce partial melts to the pelitic quartzite and the calc-silicate rocks.

Experimental partial melting studies (e.g., Holtz and Johannes 1991; Patiño-Douce and Johnston 1991; Montel and Vielzeuf 1997; Patiño-Douce and Harris 1998)

of melt generation in pelitic rocks combined with geochemical studies of migmatized aureoles surrounding plutons (e.g., Bea et al. 1994; Whitney and Irving 1994; Carrington and Watt 1995; Symmes and Ferry 1995; Zeng et al. 2005a) provide detailed information on melting reactions that are likely to occur during contact metamorphism of pelitic material, and the range of compositions that will be produced from these partial melting reactions (Figs. 4 and 7). Experimental studies and leucosome analysis define a high-K_2O initial partial melt that is indistinguishable from peraluminous leucogranite compositions (Montel and Vielzeuf 1997). In addition to the common high-K_2O partial melt, melting experiments frequently produce low-K_2O glass compositions and migmatite studies in contact aureoles have identified low-K_2O leucosomes.

Variability in potassium relates to the activity of H_2O. As the activity of H_2O increases, the melting temperature decreases and plagioclase and quartz are consumed in greater proportion than muscovite because mica stability extends to lower temperatures (Patiño-Douce and Harris 1998; Zeng et al. 2005a). Patiño-Douce and Harris (1998) conducted fluid-present and fluid-absent melting experiments on pelitic material at 0.6, 0.8, and 1.0 GPa with temperatures between 700 to 800 °C. Their results define two different melting reactions referred to below as MR-1 and MR-2. Stoichiometry in mass units was determined by the change in phase abundances at conditions that just exceed the muscovite-out boundary and the initial pelitic material.

$$22Ms + 7Pl + 8Qtz \rightarrow 25Melt + 5Kfs + 5Sil + 2Bt \quad (MR\text{-}1)$$

$$9Ms + 15Pl + 7Qtz + xH_2O \rightarrow 31Melt \quad (MR\text{-}2)$$

(Ms- muscovite, Pl- plagioclase, Qtz- quartz, Kfs- alkali feldspar, Sil- sillimanite, Bt- biotite)

The fluid absent melting reaction (MR-1) produces a melt that has greater concentrations of K_2O than the fluid-fluxed melting reaction (MR-2). Leucosomes of both varieties (high-K and low-K) occur within the same migmatite complexes (Zeng et al. 2005a), suggesting that the activity of H_2O can vary within short distances in contact aureoles. This could be related to variability in H_2O concentration, or to change in the CO_2 proportion in the fluid. As the CO_2 component of a H_2O-CO_2 fluid increases, the effectiveness of that fluid to suppress melting temperature is decreased (Ernst 1976). Free CO_2 would be available due to degassing of $CaCO_3$ found in the marble and calc-silicate rocks of the metamorphic screen.

Kga intruded at ~0.2 GPa and 720°C (Gray 2003), which is similar in temperature but significantly different in pressure conditions than the experimental results. However, these melting reactions are less sensitive to pressure changes than they are to temperature changes, and minerals and melts in the experimental results show no direct chemical correlation with pressure variations. In addition, leucosomes formed at pressures of 0.3 – 0.5 GPa and temperatures ~700°C in the southern Sierra Nevada (Zeng et al. 2005a) are consistent with the chemical reactions above. Thus, melting reactions MR-1 and MR-2 are probable simplifications of the melting dynamics of the pelitic material in the May Lake screen during emplacement of Kga.

The high concentrations of Th and LREE in some of the low-K hybrids could be related to the high dissolution rate of monazite in MR-2 (Zeng et al. 2005b). Analysis of heavy mineral separates (Table 3) suggests that monazite is the mineral with the largest concentrations of Th and LREE in the pelitic quartzite. However, the granodiorite mineral separates showed uranothorite and allanite with the largest concentrations of Th

and LREE, with the hybrid sample from within 10 cm of the pelitic quartzite containing more uranothorite and allanite than the uncontaminated granodiorite sample. It is probable that the preferential incorporation of monazite into the low-K partial melt increased the overall concentrations of LREE and Th in the adjacent hybridized magma, resulting in greater abundances of uranothorite and allanite.

Chemical data suggest that both partial melts originated from the pelitic quartzite unit in the May Lake screen. However, we have not ruled out the contribution of a calc-silicate rock partial melt. Detailed chemical studies of mafic magmas in contact with calcareous wall rocks show that basaltic magmas can initiate partial melting of the wall rocks and selectively assimilate a calcium-rich liquid (Joesten 1977; Wenzel et al. 2002), but, similar to our findings, the magma contamination is limited in extent (< 3 m; Joesten 1977), and restitic xenoliths are common (Preston et al. 1999). No calc-silicate rock xenoliths had rinds indicative of partial melting like the pelitic quartzite xenoliths. And although many of the hybridized samples are enriched in K_2O and/or Na_2O, none of the hybridized samples are enriched in CaO relative to the granodiorite.

Bulk or selective assimilation of marble and calc-silicate rocks was not observed in the plutons near May Lake and thus all incorporated calcareous material is visible as xenoliths. However, because marble and calc-silicate rocks make up a small percentage of the observed xenoliths near May Lake (<5%) and no large blocks of marble or calc-silicate rocks are observed, it is likely that little calcareous wall rock material entered the magma in any form. Because these calcareous rock types are common in the upper crust, their lack of incorporation into magma bodies inhibits the process of large-scale assimilation of metasedimentary sequences that contain marble or calc-silicate rock units.

Reconciling chemical mixing percentages

Calculated mixing percentages, from selected major-elements, of the hybridized samples cover a broad range of mixing between wall rock partial melt and magmatic (Kga) melt (Fig. 13). Major-element concentrations for Kga and the two distinct partial melts from pelitic quartzite have restricted variability and provide quantifiable mixing proportions (Table 4). However, the calculated mixing percentages for the hybrid samples have no single correlation with $^{87}Sr/^{86}Sr_{(i)}$ (Fig. 13) or $\varepsilon Nd_{(t)}$. The low correlation between calculated mixing percentages and $^{87}Sr/^{86}Sr_{(i)}$ and $\varepsilon Nd_{(t)}$ relates to: 1) the high isotopic variability of the quartzite samples ($^{87}Sr/^{86}Sr_{(i)}$ = 0.7062 to 0.7741 and $\varepsilon Nd_{(t)}$ = -5.1 to -23.7), 2) isotopic disequilibrium (Knesel and Davidson 1996; Zeng et al. 2005a) during partial melting of the pelitic material and 3) modal segregation seen in the outer portion of the pluton, which can disguise the original contamination by segregating minerals, some with drastically different distribution coefficients for Sr and Nd, with Nd especially affected by segregation of trace phases (Gromet and Silver 1983).

Mixing hyperbolas (Fig. 13) between Kga and different quartzite samples, with reasonable Sr concentrations for the partial melts (Bea et al. 1994), illustrate the high variability of $^{87}Sr/^{86}Sr_{(i)}$ that should be expected during such partial melting/ mixing processes. However, the mixing hyperbolas shown are non-quantifiable paths of mixing because multiple mixing path solutions for each hybrid sample exist. Thus the major-element mixing percentages give the more interpretable results of mixing.

Limits of contamination in the Tuolumne Intrusive Suite

The length scale of contamination along the side of the suite near May Lake is restricted to within 2 meters of wall rock material (Fig. 11). This thin rind of contamination in the outer portion of the suite can be interpreted in two ways: 1) contamination is localized at contacts between fertile wall rock and magma, and similar roof contacts in the central portions of the suite are no longer preserved owing to erosion; or 2) the identifiable chemical hybridization is only preserved at the outer contacts when and where the magma system was thermally immature, and the inner units, over time, homogenized their assimilated material such that remnants of that process are only preserved in the overall isotopic gradation from margin to core in the Tuolumne Intrusive Suite (Fig. 11).

If selective assimilation of wall rock only occurred as a rind surrounding the suite, establishing an upper limit on volume transferred from wall rock to pluton is possible. We calculated the upper limit volume percent of both Kga and the entire suite that is wall rock material by placing a 2 meter wide rind of 100% wall rock partial melt along the outer contacts with wall rock. The ~60 km^2 Kga (western, outer unit only) would thus have 0.2 area % wall rock contamination. Assuming a rectangular intrusion with roof and floor contacts contributing the same 2 m rind of contamination, and a minimum pluton thickness of 1 km (based on present relief of plutonic suite), selective assimilation could contribute 0.6 volume % of Kga. For the entire Tuolumne Intrusive Suite, selective assimilation could contribute 0.44 volume % of a 1 km thick suite. Thickening the suite decreases the percentage with a 2 km thick suite having 0.24 volume % wall rock partial melt, and a 5 km thick suite having 0.12 volume % wall rock partial melt.

If selective assimilation of wall rock was pervasive during emplacement of the Tuolumne Intrusive Suite and the increasingly crustal isotopic ratios of inner units relate to wall rock contamination, a much larger volume % wall rock partial melt is necessary in the suite. Because the major-element variability of inner units is only consistent with Kga and the high-K partial melts, there is no chemical evidence of assimilation of a low-K partial melt in the interior of the suite. Because the high-K partial melt is chemically indistinquishable from a rhyolitic melt, it is difficult to determine the origin of such a felsic contribution to the suite. However, if in situ selective assimilation is the cause, one would expect greater Sr and Nd isotopic variability in the interior of the suite due to: 1) the wall rock dependence of partial melting, and 2) the high variability in Sr and Nd isotopic ratios in the partial melts.

The systematic change in isotopic data across the entire suite (Gray 2003) suggests the Sr and Nd isotopic variability is related to an earlier stage in magma generation. A migration of the source magmatism under the Sierra Nevada batholith during the emplacement of the inner units of the suite (Gray et al. 2008), which mimics other concentrically zoned suites (e.g. Whitney Intrusive Suite; Coleman and Glazner 1997) seems a probable explanation.

Conclusions

1) The predominant observable contaminant in the outer portion of the granodiorite of Glen Aulin is pelitic quartzite, which is the only foliated metasedimentary rock unit in the adjacent May Lake metamorphic screen. This rock type makes up approximately 90% of observed xenoliths.

2) Xenoliths are exceedingly rare in the Tuolumne Intrusive Suite (<0.0001% by area; Glazner and Bartley 2008 in press), but are found in some abundance (locally up to 10% of selected 10x10 m area) in a xenolith-rich horizon subparallel to the contact. However, outside of this horizon, xenoliths make up <<1% of the exposed area, even adjacent to the contact with the metamorphic screen.

3) Major-element, trace-element, and radiogenic isotopic data suggest localized contamination of the pluton within 2 m of the contact with wall rock material.

4) No significant bulk or selective assimilation of marble or calc-silicate rocks occurred during emplacement of the granodiorite of Glen Aulin and such rocks make up only a small fraction (<10%) of observed xenoliths.

5) The contamination path is bimodal, with some of the hybridized samples trending toward high SiO_2 (~75 wt. %) and high K_2O (~5 wt. %) and the rest trending toward high SiO_2 (~75 wt. %) and low K_2O (< 1 wt. %).

6) Major-element and trace-element data suggest that bulk assimilation of wall rock was insignificant during emplacement of the Tuolumne Intrusive Suite and the localized

contaminants are partial melts selectively assimilated from the pelitic quartzite (one with high-K_2O and the other with low-K_2O).

7) Geochemical trends of contamination in the hybridized samples are consistent with data from leucosomes in migmatites which suggests that at least two main melting reactions produce two chemically distinct partial melts, one high-K_2O and one low-K_2O.

8) Assimilation of wall rock is not a significant space conserving mechanism for the emplacement of the Tuolumne Intrusive Suite because of the spatially restricted contamination of the plutonic rocks.

TABLE 1 whole-rock major-element concentrations (wt. %)

Sample Name	SiO_2	TiO_2	Al_2O_3	Fe_2O_3(T)	MnO	MgO	CaO	Na_2O	K_2O	P_2O_5	LOI	TOTAL
granodiorite												
ML051.04	67.63	0.513	15.56	3.96	0.061	1.67	3.45	3.17	4.04	0.15	0.370	100.60
ML061.61	60.23	0.741	17.35	5.96	0.099	2.54	5.50	3.69	2.71	0.22	1.159	100.20
ML061.63	61.54	0.764	16.25	5.75	0.089	2.43	4.78	3.28	3.20	0.22	1.189	99.50
hybridized granodiorite												
ML051.02	77.86	0.331	11.17	1.95	0.031	0.73	2.55	2.53	1.61	0.08	0.444	99.29
ML051.08	66.62	0.517	15.73	4.42	0.062	1.72	3.86	3.33	3.81	0.17	0.347	100.60
ML051.18	64.38	0.863	16.54	5.58	0.068	2.45	4.39	3.41	2.28	0.23	0.506	100.70
ML061.25	66.56	0.852	15.67	4.62	0.053	1.95	4.10	3.40	2.10	0.19	1.075	100.60
ML061.26	62.06	0.785	16.74	5.89	0.088	2.49	5.01	3.46	3.04	0.23	0.905	100.70
ML061.28	76.69	0.137	12.81	1.17	0.020	0.34	1.90	2.65	4.36	0.06	0.392	100.50
ML061.30	72.00	0.194	15.43	1.61	0.031	0.50	2.77	3.43	4.03	0.08	0.448	100.50
ML061.32	61.29	1.869	13.00	10.14	0.153	4.09	2.19	2.01	3.74	0.40	1.213	100.10
ML061.36	75.68	0.393	12.49	2.32	0.029	1.05	2.64	2.13	2.05	0.05	1.426	100.30
ML061.38	64.88	0.975	14.97	6.29	0.107	2.74	3.23	2.23	3.43	0.26	1.325	100.40
ML061.40	67.49	0.591	14.78	4.35	0.054	1.61	3.07	2.93	3.60	0.15	1.157	99.79
ML061.60	72.59	0.410	13.93	2.67	0.043	1.22	3.64	3.12	1.17	0.08	1.153	100.00
quartzite												
ML051.14	91.61	0.064	4.64	1.20	0.021	0.54	0.18	0.15	1.31	0.09	0.368	100.20
ML061.24	88.79	0.103	5.81	0.91	0.006	0.10	0.27	0.79	3.22	0.04	0.492	100.50
ML061.37	89.14	0.195	5.81	0.47	0.011	0.10	0.27	0.83	3.26	0.02	0.319	100.40
ML061.39	94.82	0.083	2.13	0.73	0.006	0.14	0.09	0.24	0.90	0.04	0.442	99.63
pelitic quartzite												
ML051.03	81.44	0.600	7.68	3.48	0.054	1.34	0.92	1.30	2.90	0.14	0.348	100.20
ML061.29	67.30	0.791	15.93	3.86	0.130	1.81	7.14	1.22	1.15	0.10	1.134	100.60
calc-silicate rocks												
ML051.17	48.74	0.511	14.52	7.73	0.440	6.18	21.68	0.39	0.07	0.10	0.239	100.10
ML061.59	50.93	0.665	15.94	6.14	0.356	8.42	15.82	0.47	0.52	0.09	1.024	100.40
marbles												
ML051.05	34.83	0.028	0.59	1.02	0.200	1.54	47.47	0.02	< 0.01	0.97	13.910	100.60
ML-85	15.11	0.061	0.82	0.88	0.061	4.35	48.00	0.02	0.02	0.07	31.240	100.60
pelitic xenolith												
ML051.09	59.28	0.742	17.57	6.73	0.125	3.60	5.61	3.40	2.09	0.27	0.544	99.97

TABLE 1 (cont.) whole-rock trace-element concentrations (ppm)

Sample Name	Sc	Be	V	Cr	Co	Ni	Cu	Zn	Ga	Ge	As	Rb	Sr	Y	Zr	Nb	Mo	Ag	In	Sn	Sb	Cs
granodiorite																						
ML051.04	6	2	77	< 20	9	< 20	< 10	50	16	1.1	< 5	172	422	8.0	156	4.5	< 2	< 0.5	< 0.1	< 1	0.4	7.8
ML061.61	12	2	123	< 20	14	< 20	< 10	70	21	1.3	5	131	523	32.2	191	8.8	< 2	< 0.5	< 0.1	2	< 0.2	9.2
ML061.63	11	2	124	< 20	14	< 20	< 10	70	19	1.3	6	150	500	18.6	165	6.9	< 2	< 0.5	< 0.1	1	0.8	7.2
hybridized granodiorite																						
ML051.02	2	1	41	< 20	5	< 20	20	< 30	12	0.9	6	90	261	6.9	350	3.2	< 2	< 0.5	< 0.1	< 1	0.4	6.9
ML051.08	12	2	87	< 20	8	< 20	30	50	16	1.1	5	141	435	30.2	157	7.7	< 2	< 0.5	< 0.1	< 1	0.4	6.7
ML051.18	7	2	129	< 20	12	< 20	20	60	19	1.0	< 5	168	411	5.1	198	8.1	< 2	< 0.5	< 0.1	< 1	0.6	13.4
ML061.25	4	2	117	< 20	10	< 20	40	60	17	0.9	< 5	134	439	15.4	150	8.2	< 2	< 0.5	< 0.1	1	0.4	7.7
ML061.26	11	2	125	< 20	13	< 20	20	60	18	1.0	< 5	141	508	9.6	165	5.3	< 2	< 0.5	< 0.1	< 1	0.4	7.3
ML061.28	1	1	21	< 20	2	< 20	< 10	< 30	11	1.0	< 5	122	352	3.5	77	2.5	< 2	< 0.5	< 0.1	< 1	0.3	8.3
ML061.30	1	1	25	< 20	4	< 20	< 10	970	16	1.1	< 5	130	466	2.8	91	3.0	< 2	< 0.5	< 0.1	< 1	< 0.2	6.9
ML061.32	17	2	206	< 20	23	< 20	< 10	140	24	1.9	< 5	316	159	37.1	311	32.2	< 2	< 0.5	< 0.1	3	4.6	23.2
ML061.36	6	1	43	< 20	7	< 20	< 10	< 30	15	1.1	< 5	83	215	13.7	169	9.3	3	< 0.5	< 0.1	< 1	< 0.2	3.6
ML061.38	13	1	151	< 20	14	< 20	< 10	80	21	1.4	6	256	155	22.5	201	17.6	4	< 0.5	< 0.1	3	0.3	18.1
ML061.40	3	2	90	< 20	9	< 20	< 10	50	18	1.0	< 5	175	356	3.8	177	3.6	< 2	< 0.5	< 0.1	< 1	< 0.2	8.2
ML061.60	4	2	46	< 20	7	< 20	30	40	17	1.1	< 5	109	318	4.5	175	6.8	< 2	< 0.5	< 0.1	< 1	< 0.2	12.7
quartzite																						
ML051.14	1	< 1	6	< 20	3	< 20	< 10	< 30	5	1.0	23	25	18	12.6	31	1.1	< 2	< 0.5	< 0.1	< 1	0.3	1.0
ML061.24	< 1	< 1	17	< 20	1	< 20	20	< 30	5	0.7	< 5	89	190	3.4	362	1.4	< 2	< 0.5	< 0.1	< 1	0.4	2.4
ML061.37	1	< 1	11	< 20	< 1	< 20	< 10	< 30	5	0.9	< 5	97	45	2.8	161	4.2	6	< 0.5	< 0.1	< 1	< 0.2	3.3
ML061.39	< 1	< 1	13	< 20	3	< 20	60	< 30	3	0.7	5	33	24	3.9	359	1.3	< 2	< 0.5	< 0.1	< 1	3.9	1.5
pelitic quartzite																						
ML051.03	6	1	38	40	5	20	10	30	10	0.9	< 5	123	30	26.8	507	8.2	< 2	< 0.5	< 0.1	< 1	0.3	8.3
ML061.29	11	2	78	80	2	< 20	60	40	18	1.0	26	61	108	19.3	190	14.0	< 2	< 0.5	< 0.1	< 1	0.3	6.0
calc-silicate rocks																						
ML051.17	13	3	61	60	11	30	60	130	19	1.5	12	8	151	34.2	150	13.4	2	< 0.5	< 0.1	6	0.8	1.7
ML061.59	14	3	80	80	9	40	< 10	80	23	2.1	< 5	33	214	37.4	166	14.8	< 2	< 0.5	< 0.1	2	< 0.2	1.8
marbles																						
ML051.05	< 1	< 1	27	< 20	< 1	< 20	< 10	< 30	1	< 0.5	47	< 1	94	8.6	12	2.0	< 2	< 0.5	< 0.1	< 1	0.7	< 0.1
ML-85	1	< 1	6	< 20	< 1	< 20	< 10	< 30	1	< 0.5	< 5	< 1	279	5.9	106	1.8	< 2	< 0.5	< 0.1	< 1	0.4	0.1
pelitic xenolith																						
ML051.09	21	2	92	90	13	< 20	< 10	80	18	1.4	< 5	68	745	24.5	129	8.6	< 2	< 0.5	< 0.1	1	0.6	5.2

TABLE 1 (cont.) whole-rock trace-element concentrations (ppm)

Sample Name	Ba	La	Ce	Pr	Nd	Sm	Eu	Gd	Tb	Dy	Ho	Er	Tm	Yb	Lu	Hf	Ta	W	Tl	Pb	Bi	Th	U
granodiorite																							
ML051.04	993	14.9	28	2.78	9.91	1.84	0.67	1.49	0.24	1.33	0.26	0.77	0.13	0.88	0.15	4.2	0.43	< 0.5	0.91	28	0.1	55.3	12.4
ML061.61	824	24.7	61.6	7.62	30.7	6.36	1.46	5.37	0.94	5.28	1.02	3.16	0.51	3.36	0.48	5.5	1.65	1.1	0.7	13	0.2	22.7	9.67
ML061.63	861	26.6	55.1	5.95	22.8	4.32	1.12	3.5	0.58	3.25	0.63	1.79	0.26	1.63	0.25	4.8	0.56	0.7	0.82	14	0.2	30.9	8.11
hybridized granodiorite																							
ML051.02	275	122	213	18.8	57.6	6.09	0.8	3.34	0.32	1.4	0.24	0.71	0.11	0.76	0.14	9.6	0.3	0.5	0.51	13	0.2	74.6	12.1
ML051.08	1125	15.6	40.2	5.47	24.4	5.91	1.05	5.28	0.93	5.42	1.01	2.84	0.42	2.57	0.37	4.6	0.8	< 0.5	0.78	15	0.1	29.4	5.82
ML051.18	326	32.7	56.9	5.49	17.4	2.34	1.04	1.69	0.21	0.99	0.18	0.51	0.07	0.51	0.09	5.2	0.34	2.7	1.04	10	0.1	13.1	4.39
ML061.25	379	28.2	52.4	6.37	23.5	4.11	1.3	3.36	0.51	2.65	0.49	1.46	0.22	1.39	0.22	4.3	1.59	3.4	0.8	10	0.2	17	7.73
ML061.26	858	19	36.6	3.71	13.1	2.48	0.86	2.03	0.32	1.81	0.34	0.96	0.14	0.97	0.15	4.5	0.38	4.6	0.75	17	0.9	18.6	5.19
ML061.28	1127	8.52	12.6	1.08	3.43	0.56	0.38	0.45	0.08	0.52	0.11	0.35	0.06	0.48	0.08	2.6	0.37	< 0.5	0.66	21	0.1	11.4	4.54
ML061.30	1054	12.9	18.1	1.42	4.26	0.66	0.49	0.42	0.07	0.41	0.08	0.26	0.04	0.35	0.06	2.8	0.3	< 0.5	0.64	21	0.2	21.7	5.28
ML061.32	259	200	330	31.1	106	15.9	1.29	10.8	1.52	7.58	1.28	3.32	0.43	2.47	0.34	9.5	4.67	< 0.5	1.82	7	0.2	119	14.2
ML061.36	330	62.1	127	13.2	47.7	7.65	1.17	5.48	0.75	3.21	0.5	1.17	0.14	0.76	0.1	5.3	0.64	1	0.47	15	< 0.1	59.4	3.36
ML061.38	358	14.9	32.2	3.68	15.1	3.53	0.89	3.32	0.64	4.02	0.78	2.26	0.33	2.05	0.3	5.6	1.19	3.3	1.74	15	0.1	8.48	2.96
ML061.40	640	10.4	17.4	1.75	6.68	1.19	0.62	0.97	0.14	0.72	0.13	0.36	0.05	0.37	0.06	5.2	0.13	< 0.5	0.94	15	< 0.1	29.1	5.13
ML061.60	131	12.9	19.2	1.96	6.51	1.04	0.69	0.85	0.13	0.73	0.15	0.44	0.07	0.53	0.09	5.7	0.6	< 0.5	0.62	9	0.1	34.7	13.4
quartzite																							
ML051.14	195	10.5	22.7	2.39	9.06	1.92	0.51	1.82	0.34	2.08	0.43	1.31	0.2	1.28	0.19	0.9	0.16	< 0.5	0.16	< 5	0.6	2.78	2.25
ML061.24	989	26.8	49.6	4.53	13.5	1.57	0.32	0.87	0.11	0.56	0.11	0.39	0.07	0.57	0.11	9.6	0.42	< 0.5	0.43	12	< 0.1	25.2	5.17
ML061.37	382	7.92	14.3	1.38	4.56	0.72	0.37	0.5	0.08	0.42	0.09	0.28	0.05	0.35	0.06	4.4	0.35	2.8	0.47	19	0.1	9.68	2.81
ML061.39	94	23.6	44.8	3.98	13.1	1.63	0.15	1.03	0.14	0.67	0.13	0.41	0.07	0.52	0.1	11.8	0.09	0.5	0.21	5	0.1	127	19.1
pelitic quartzite																							
ML051.03	312	42.4	101	9.97	37.1	6.86	1.22	5.89	0.94	4.94	0.93	2.73	0.38	2.35	0.37	12.2	0.69	1.2	0.74	9	< 0.1	18.7	2.01
ML061.29	130	16.8	42.1	4.65	19.3	4.32	1.13	4.1	0.73	4	0.71	1.93	0.26	1.6	0.24	5	1.42	< 0.5	0.41	6	< 0.1	10.5	2.28
calc-silicate rocks																							
ML051.17	22	36.5	85.3	9.54	37	7.28	1.86	6.64	1.13	6.22	1.15	3.21	0.47	2.98	0.45	3.9	1.23	19.3	< 0.05	< 5	0.2	10.2	4.65
ML061.59	337	52.1	107	11.5	42.4	7.62	1.58	6.51	1.14	6.38	1.24	3.74	0.58	3.7	0.52	4.9	1.38	< 0.5	0.17	< 5	0.2	16.6	3.35
marbles																							
ML051.05	8	5.27	7.93	1.04	4.03	0.74	0.3	0.77	0.12	0.69	0.15	0.49	0.07	0.45	0.07	0.3	0.11	< 0.5	< 0.05	8	6.4	0.9	9.82
ML-85	16	5.59	13.3	1.31	4.93	1.02	0.26	0.89	0.16	0.94	0.18	0.55	0.09	0.59	0.1	2.7	0.11	1	< 0.05	8	< 0.1	2.52	1.48
pelitic xenolith																							
ML051.09	752	24.4	50.9	5.76	22.7	4.69	1.45	4.18	0.72	4.24	0.84	2.48	0.37	2.43	0.38	3.3	0.78	1.3	0.6	13	0.2	6.7	2.28

TABLE 2 whole-rock Sr and Nd isotopic data

Sample Name	$^{143}Nd/^{144}Nd$	± 2s	$\mu Nd_{(t)}$	[Nd]	[Sm]	$^{87}Sr/^{86}Sr$	± 2s	$^{87}Sr/^{86}Sr_i$	[Sr]	[Rb]
granodiorite										
ML051.04	0.512410	0.000012	-3.45	9.9	1.8	0.707384	0.000008	0.705802	422	172
ML061.61	0.512405	0.000009	-3.70	30.7	6.4	0.706907	0.000010	0.705935	523	131
ML061.63	0.512394	0.000010	-3.78	22.8	4.3	0.706959	0.000007	0.705795	500	150
hybridized granodiorite										
ML051.02	0.512286	0.000012	-5.29	57.6	6.1	0.707678	0.000008	0.706340	261	90
ML051.08	0.512403	0.000008	-3.99	24.4	5.9	0.707363	0.000007	0.706105	435	141
ML051.18	0.512273	0.000010	-5.75	17.4	2.3	0.708775	0.000006	0.707189	411	168
ML061.25	0.512400	0.000007	-3.56	23.5	4.1	0.707818	0.000008	0.706633	439	134
ML061.26	0.512428	0.000044	-3.13	13.1	2.5	0.707569	0.000007	0.706492	508	141
ML061.28	0.512240	0.000023	-6.61	3.4	0.6	0.707823	0.000008	0.706478	352	122
ML061.30	0.512257	0.000014	-6.20	4.3	0.7	0.707307	0.000009	0.706224	466	130
ML061.32	0.512230	0.000022	-6.70	106.0	15.9	0.714813	0.000006	0.707100	159	316
ML061.36	0.512089	0.000006	-9.52	47.7	7.7	0.715645	0.000007	0.714147	215	83
ML061.38	0.512067	0.000006	-10.48	15.1	3.5	0.717084	0.000007	0.710674	155	256
ML061.40	0.512341	0.000013	-4.73	6.7	1.2	0.708109	0.000007	0.706201	356	175
ML061.60	0.512179	0.000097	-7.76	6.5	1.0	0.708401	0.000007	0.707071	318	109
quarzite										
ML051.14	0.511475	0.000023	-21.89	9.1	1.9	0.765441	0.000007	0.760051	18	25
ML061.24	0.512299	0.000007	-5.10	13.5	1.6	0.708037	0.000008	0.706219	190	89
ML061.37	0.511646	0.000028	-18.15	4.6	0.7	0.722843	0.000007	0.714478	45	97
ML061.39	0.512157	0.000007	-7.95	13.1	1.6	0.711588	0.000007	0.706252	24	33
pelitic quartzite										
ML051.03	0.511373	0.000010	-23.67	37.1	6.9	0.789945	0.000007	0.774034	30	123
ML061.29	0.511917	0.000048	-13.35	19.3	4.3	0.732385	0.000007	0.730193	108	61
calc-silicate rocks										
ML051.17	0.511635	0.000025	-18.65	37.0	7.3	0.728369	0.000007	0.728164	151	8
ML061.59	0.511625	0.000008	-18.72	42.4	7.6	0.748255	0.000008	0.747656	214	33
marbles										
ML051.05				4.0	0.7	0.710385	0.000007	0.710344	94	1
ML-85	0.511750	0.000018	-16.47	4.9	1.0	0.710961	0.000007	0.710947	279	1
pelitic xenolith										
ML051.09	0.512277	0.000009	-6.20	22.7	4.7	0.707237	0.000007	0.706883	745	68

TABLE 3 heavy mineral separates mineral data

	pelitic quartzite ML051.03	hybridized granodiorite ML051.02	granodiorite ML061.63
Monazite percent of heavy minerals	~10%		
Uranothorite percent of heavy minerals		~3%	<1%
Allanite percent of heavy minerals		~15%	<1%
Ce in monazite (ppm)	~15		
Th in monazite (ppm)	~3		
Ce in allanite (ppm)		~18	<3
Th in uranothorite (ppm)		~27	<18
Ce in whole-rock (ppm)	101	213	55
Th in whole-rock (ppm)	19	75	31
heavy minerals/total	0.05 wt.%	0.2 wt.%	0.4 wt.%

Heavy mineral separates contain minerals that passed through MEI liquid with a density of 3.2 g/cm^3. Mineral percentages were estimated by point counts of heavy mineral mounts using energy dispersive spectrometry (EDS) on a SEM.

TABLE 4 weighted least squares results of mixing

Oxide	Kga	partial melt	low-K hybridized granodiorite					partial melt	high-K hybridized granodiorite					weights (1/)
	ML061.63	low-K	ML051.02	ML051.18	ML061.60	ML061.25	ML061.36	high-K	ML061.28	ML061.30	ML061.38	ML051.08	ML061.40	
SiO_2	61.54	76.00	77.86	64.38	72.59	66.56	75.68	74.89	76.69	72.00	64.88	66.62	67.49	4.9
TiO_2	0.76	0.15	0.33	0.86	0.41	0.85	0.39	0.11	0.14	0.19	0.98	0.52	0.59	88.5
Al_2O_3	16.25	12.50	11.17	16.54	13.93	15.67	12.49	14.15	12.81	15.43	14.97	15.73	14.78	5.2
MgO	2.43	0.50	0.73	2.45	1.22	1.95	1.05	0.33	0.34	0.50	2.74	1.72	1.61	17.5
CaO	4.78	2.95	2.55	4.39	3.64	4.10	2.64	0.91	1.90	2.77	3.23	3.86	3.07	24.9
Na_2O	3.28	4.00	2.53	3.41	3.12	3.40	2.13	2.79	2.65	3.43	2.23	3.33	2.93	15.9
K_2O	3.20	0.50	1.61	2.28	1.17	2.10	2.05	5.07	4.36	4.03	3.43	3.81	3.60	25.2
partial melt component			**1.00**	**0.13**	**0.69**	**0.29**	**0.87**		**1.00**	**0.61**	**0.32**	**0.30**	**0.46**	
Kga component			**-0.08**	**0.89**	**0.32**	**0.72**	**0.13**		**0.00**	**0.42**	**0.66**	**0.72**	**0.53**	

Fe oxide concentrations omitted due to the variability of technique and reporting style

References

Barnes CG, Dumond G, Yoshinobu AS, Prestvik T (2004) Assimilation and crystal accumulation in a mid-crustal magma chamber: the Sausfjellet pluton, north-central Norway. Lithos 75:389-412

Barnes CG, Prestvik T, Sundvoll B, Surratt D (2005) Pervasive assimilation of carbonate and silicate rocks in the Hortavær igneous complex, north-central Norway. Lithos 80:179-199

Bateman PC, Chappell BW (1979) Crystallization, fractionation, and solidification of the Tuolumne intrusive series, Yosemite National Park, California. Geological Society of American Bulletin 90:465-482

Bateman PC, Chappell BW, Kistler RW, Peck DL, Busacca AJ (1988) Tuolumne Meadows Quadrangle, California; analytic data, U. S. Geological Survey Bulletin, Report: B 1819 8755-531X

Bea F, Pereira MD, Stroh A (1994) Mineral/leucosome trace-element partitioning in a peraluminous migmatite (a laser ablation-ICP-MS study). Chemical Geology 117:291-312

Beard JS, Ragland PC, Crawford ML (2005) Reactive bulk assimilation: A model for the crust-mantle mixing in silicic magmas. Geology 33:681-684

Bowen NL (1928) The evolution of igneous rocks: Princeton, New Jersey, Princeton University Press, p 332

Carrington DP, Watt GR (1995) A geochemical and experimental study of the role of K-feldspar during water-undersaturated melting of metapelites. Chemical Geology 122:59-76

Clarke FW (1908) The Data of Geochemistry: U.S. Geological Survey Bulletin No. 330, p 716

Clarke DB, Henry AS, White MA (1998) Exploding xenoliths and the absence of "elephants' graveyards" in granite batholiths. Journal of Structural Geology 20:1325-1343

Coleman DS, Glazner AF (1997) The Sierra Crest magmatic event: rapid formation of juvenile crust during the late Cretaceous in California. International Geology Review 39:768-787

Coleman DS, Gray W, Glazner AF (2004) Rethinking the emplacement and evolution of zoned plutons: Geochronologic evidence for incremental assembly of the Tuolumne Intrusive Suite, California. Geological Society of America Bulletin 32:433-436

Coleman DS, Glazner AF, Bartley JM, Law RD (2005) Incremental assembly and emplacement of Mesozoic plutons in the Sierra Nevada and White and Inyo Ranges, California: Geological Society of America Field Forum Field Trip Guide (Rethinking the assembly and evolution of plutons: Field tests and perspectives, 7-14 October 2005) p 55

Dungan MA (2005) Partial melting at the earth's surface: implications for assimilation rates and mechanisms in subvolcanic intrusions. Journal of Volcanology and Geothermal Research 140:193–203

Ernst (1976) Petrologic phase equilibria: San Francisco, California, W.H. Freeman and Company, 333 p

Glazner AF, Bartley JM (2006) Is stoping a volumetrically significant pluton emplacement process? Geological Society of America Bulletin 118:1185-1195

Glazner AF (2007) Thermal limitations on incorporation of wall rock into magma. Geology 35:319-322

Glazner AF, Bartely JM (2008) Reply to comments on "Is stoping a volumetrically significant pluton emplacement process?" Geological Society of America Bulletin, in press

Gray W, Glazner AF, Coleman DS, Bartley JM (2008) Long-term geochemical variability of the Late Cretaceous Tuolumne Intrusive Suite, Central Sierra Nevada, California. Geological Society of London, Special Paper, in press

Gray W (2003) Chemical and thermal evolution of the Late Cretaceous Tuolumne intrusive suite, Yosemite National Park, California [Ph.D. thesis]: Chapel Hill, North Carolina, University of North Carolina, p 202

Gromet LP, Silver LT (1983) Rare earth element distributions among minerals in a granodiorite and their petrogenetic implications. Geochemica et Cosmochimica Acta 47:925-939

Holtz F, Johannes W (1991) Genesis of peraluminous granites I. Experimental investigation of melt compositions at 3 and k kb and various H_2O activities. Journal of Petrology 32:935-958

Huber NK, Bateman PC, Wahrhaftig C (1989) Geologic map of Yosemite National Park and vicinity, California: U.S. Geological Survey Map I-1874, scale 1:125,000

Joesten R (1977) Mineralogical and chemical evolution of contaminated igneous rocks at a gabbro-limestone contact, Christmas Mountains, Big Bend region, Texas. Geological Society of America Bulletin 88:1515-1529

Kistler RW, Chappell BW, Peck DL, Bateman PC (1986) Isotopic variations in the Tuolumne Intrusive Suite, central Sierra Nevada, California. Contributions to Mineralogy and Petrology 94:205-220

Knesel,KM, Davidson JP (1996) Isotopic disequilibrium during melting of granite and implications for crustal contamination of magmas. Geology 24:243-246

Lahren MM, Schweickert RA, Mattinson JM, Walker JD (1990) Evidence of uppermost Proterozoic to Lower Cambrian miogeoclinal rocks and the Mojave-Snow Lake fault: Snow Lake pendant, central Sierra Nevada, California. Tectonics 9:1585-1608

Le Maitre RW (2002) Igneous Rocks: A Classification and Glossary of Terms, 2nd ed. Cambridge, Cambridge University Press, p 236

McBirney AR, Taylor HP, Armstrong RL (1987) Paricutin re-examined: a classic example of crustal assimilation in calc-alkaline magma. Contributions to Minealogy and Petrology 95: 4-20

Miller JS, Glazner AF, Walker JD, Martin MW (1995) Geochronologic and isotopic evidence for Triassic-Jurassic emplacement of the eugeoclinal allochthon in the Mojave Desert region, California. Geologic Society of America Bulletin 107:1441-1457

Montel JM, Vielzeuf D (1997) Partial melting of metagreywackes, Part II. Compositions of minerals and melts. Contributions to Mineralogy and Petrology 128:176-196

Otamendi JE, Patiño-Douce AE (2001) Partial melting of aluminous metagreywackes in the Northern Sierra de Comechingones, Central Argentina. Journal of Petrology 42:1751-1772

Paterson SR, Fowler Jr. TK, Miller RB (1996) Pluton emplacement in arcs: a crustal-scale exchange process. Transactions of the Royal Society of Edinburgh: Earth Science 87:115-123

Patiño-Douce AE, Johnston AD (1991) Phase equilibria and melt productivity in the pelitic system: implications for the origin of peraluminous granitoids and aluminous granulites. Contributions to Mineralogy and Petrology 107:202-218

Patiño-Douce AE, Harris N (1998) Experimental constraints on Himalayan anatexis. Journal of Petrology 39:689-710

Preston RJ, Dempster TJ, Bell BR, Rogers G (1999) The petrology of mullite-bearing peraluminous xenoliths: implications for contamination processes in basaltic magmas. Journal of Petrology 40:549-573

Rose RL (1957) Andalusite and corundum bearing pegmatities in Yosemite National Park, California. American Mineralogist 42:635-647

Saito S, Makoto A, Nakajima T (2007) Hybridization of a shallow 'I-type' granitoid pluton and its host migmatite by magma-chamber wall collapse: the Tokuwa Pluton, Central Japan. Journal of Petrology 48:79-111

Schweickert RA, Lahren MM (1991) Age and tectonic significance of metamorphic rocks along the axis of the Sierra Nevada batholith: a critical reappraisal. In: Cooper J, Stevens C (eds) Paleozoic paleography of the western United States-II: Society for Sedimentary Geology, Pacific Section 67:653-676

Sun SS, McDonough WF (1989) Chemical and isotopic systematics of oceanic basalts; implications for mantle composition and processes. Geological Society of London Special Publications 42:313-345

Symmes GH, Ferry JM (1995) Metamorphism, fluid flow and partial melting in pelitic rocks from the Onawa contact aureole, Central Maine, USA. Journal of Petrology 36:587-612

Taylor RZ (2003) Structure and stratigraphy of the May Lake interpluton screen, Yosemite National Park, California [M.S. thesis]: Chapel Hill, North Carolina, University of North Carolina, p 55

Verplank PL, Farmer G.L, McCurry M, Mertzman SA (1999) The chemical and isotopic differentiation of an epizonal magma body: Organ Needle Pluton, New Mexico. Journal of Petrology 40:653-678

Wenzel T, Baumgartner LP, Brugmann GE, Konnikov EG, Kislov EV (2002) Partial melting and assimilation of dolomitic xenoliths by mafic magma: the Ioko-Dovyren intrusion (North Baikal Region, Russia). Journal of Petrology 43:2049-2074

Whitney DL, Irving AJ (1994) Origin of K-poor leucosomes in a metasedimentary migmatite complex by ultrametamorphism, syn-metamorphic magmatism and subsolidus processes. Lithos 32:173-192

Zeng L, Saleeby JB, Ducea M (2005a) Geochemical characteristics of crustal anatexis during the formation of migmatite at the Southern Sierra Nevada, California. Contributions to Mineralogy and Petrology 150:386-402

Zeng L, Asimow PD, Saleeby JB (2005b) Coupling of anatectic reactions and dissolution of accessory phases and the Sr and Nd isotope systematic of anatectic melts from a metasedimentray source. Geochemica et Cosmochimica Acta 69:3671-3682